



Lawrence Berkeley Laboratory

UNIVERSITY OF CALIFORNIA

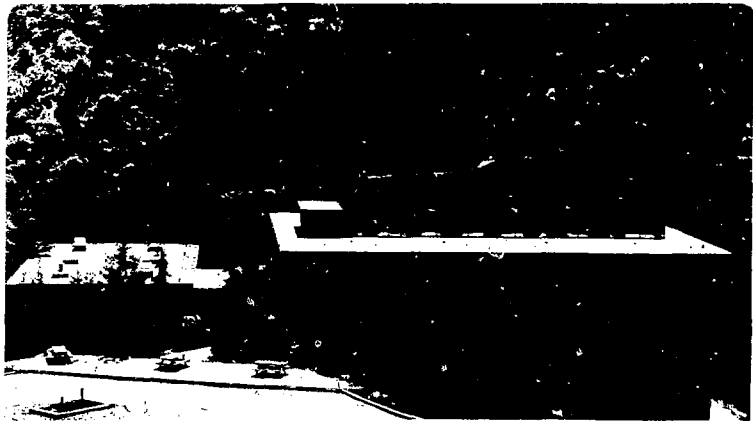
Materials & Molecular Research Division

PRECISE MEASUREMENT OF PARITY NONCONSERVATION
IN ATOMIC THALLIUM

Larry Russel Hunter
(Ph.D. thesis)

May 1981

MASTER



Prepared for the U.S. Department of Energy under Contract W-7405-ENG-48

PRECISE MEASUREMENT OF PARITY NONCONSERVATION
IN ATOMIC THALLIUM

Larry Russel Hunter

Materials and Molecular Research Division
Lawrence Berkeley Laboratory
University of California
Berkeley, California 94720

Ph.D. Thesis

May 1981

DISCLAIMER

This book was prepared as an account of work sponsored by an agency of the United States Government. Neither the United States Government nor any agency thereof, nor any of their employees, makes any warranty, expressed or implied, or assumes any legal liability or responsibility for the accuracy, completeness, or usefulness of any information, apparatus, product, or process disclosed, or represents that its use would not infringe privately owned rights. Reference herein to any specific commercial product, process, or service by trade name, trademark, manufacturer, or otherwise, does not necessarily constitute or imply its endorsement, recommendation, or favoring by the United States Government or any agency thereof. The views and opinions of authors expressed herein do not necessarily state or reflect those of the United States Government or any agency thereof.

This work was supported by the Chemical Sciences Division,
Office of Basic Energy Sciences, U. S. Department of Energy, under
Contract No. W-7405-ENG-48, through the Materials and Molecular Research
Division of the Lawrence Berkeley Laboratory.

UNCLASSIFIED
1-16-01

ACKNOWLEDGEMENTS

I wish to thank for their invaluable contributions to this research:

Eugene Commins, who has been the ideal mentor and a continuous source of inspiration.

Philip Bucksbaum, who has worked closely with me during the last three years.

David Neuffer, who introduced me to heavy atom atomic theory and some enjoyable irish songs.

Ralph Conti, for his inspired idea utilized to analyze the $7P_{1/2}$ polarization.

Steve Chu, who designed and built our lasers and pirated the key to the machine shop.

Lucien Roesch, who assisted in the most recent stages of this work and is inadvertantly preparing me for my European visit.

Persis Drell, for assistance.

Bob Hamilton, for excellent glass blowing.

Roger Koch, whose extensive computer knowledge made it possible for me to avoid R.T.S.

Alan George, for helping me clarify and articulate some vague intuitions.

Walter Knight, for his enthusiasm and support.

The Atomic Physics Group, particularly Mike Prior, Richard Marrus, and Howard Shugart.

Diana Morris, for typing this manuscript.

I wish also to thank Ulla Commins for encouragement and Susan for her love, tolerance, and support.

This thesis is dedicated to my father, Max B. Hunter.

This work was supported by the Chemical Sciences Division, Office of Basic Energy Sciences, U.S. Department of Energy, under Contract No. W-7405-ENG-48, through the Molecular Materials Research Division of the Lawrence Berkeley Laboratory.

Table of Contents

I. Introduction	1
A. Weak Neutral Currents	1
B. Parity Non-conservation in Atoms	4
C. Parity Non-conservation in Thallium	7
II. Semi-Empirical Determination of δ	10
A. General Description of Method	10
B. Measurement of the $7P_{1/2}$ lifetime	12
C. Measurement of the $7P_{3/2}$ lifetime	16
D. Measurement of $A(7^2P_{1/2}-6^2D_{3/2})$	19
E. Determination of α , β , M , ϵ_p , and δ	25
III. Description of the Experiment to Measure δ	29
A. Experimental Method and Apparatus	29
B. Selective Excitation and Analyzing Power	39
IV. Analysis of Systematic Errors and Corrections	42
A. General Remarks	42
B. Data Collection	43
C. The Effects of Imperfect UV Circular Polarization	45
D. The Effects of Stray Electric and Magnetic Fields and Their Couplings to Polarization Imperfections	47
E. Methods of Measuring False Parity Effects	50
1. Information in Parity Data	50
2. Measurements with Linearly Polarized UV	50
3. Measurements Employing Magnetic Fields and Circularly Polarized Light	52

V. Data Analysis and Results	54
A. Secondary Data Sets and Auxiliary Data.	54
B. Results	59
C. Correlation Tests	62
D. Systematic Uncertainties and Final Results.	62
VI. Comparison to Other Experiments and Theories.	65
VII. Conclusions	69
VIII. Future Work	72
References.	73

PRECISE MEASUREMENT OF PARITY NONCONSERVATION
IN ATOMIC THALLIUM

Materials and Molecular Research Division
Lawrence Berkeley Laboratory
University of California
Berkeley, California 94720

Larry R. Hunter

ABSTRACT

Observation of parity non-conservation in the $6P_{1/2} - 7P_{1/2}$ transition in $^{203,205}_{81}\text{Tl}$ is reported. The transition is nominally forbidden M1 with amplitude M. Due to the violation of parity in the electron-nucleon interaction, the transition acquires an additional (parity nonconserving) amplitude ϵ_p . In the presence of an electric field, incident 293 nm circularly polarized light results in a polarization of the $7P_{1/2}$ state through interference of the Stark amplitude with M and ϵ_p . This polarization is observed by selective excitation of the $7P_{1/2} - 8S_{1/2}$ transition with circularly polarized 2.18 μ light and observation of the subsequent fluorescence at 323 nm. By utilizing this technique and carefully determining possible systematic contributions through auxiliary measurements, the circular dichroism

$\delta = \frac{2\text{Im}(\epsilon_p)}{M}$ is observed:

$$\delta_{\text{exp}} = (2.8 \begin{matrix} +1.0 \\ -.9 \end{matrix}) \times 10^{-3}.$$

In addition, measurements of $A(6D_{3/2} - 7P_{1/2}) = (5.97 \pm .78) \times 10^5 \text{ s}^{-1}$, $A(7P_{1/2} - 7S_{1/2}) = (1.71 \pm .07) \times 10^7 \text{ s}^{-1}$ and $A(7P_{3/2} - 7S_{1/2}) = (2.37 \pm .09) \text{ s}^{-1}$ are reported. These values are employed in a semi-empirical determination of s based on the Weinberg-Salam Model. The result of this calculation for $\sin^2 \theta_w = .23$ is $\delta_{\text{Theo}} = (1.7 \pm .8) \times 10^{-3}$.

I. INTRODUCTION

A. Weak Neutral Currents

The Unified nonabelian gauge theory of the weak and electromagnetic interaction (Wei 67, Sal 68), unlike the old Fermi model of weak interactions, is renormalizable and does not violate unitarity. The theory predicts the existence of a weak neutral current (coupled to a neutral Intermediate Vector Boson, the Z_0), in addition to the familiar charged weak currents (coupled to the charged Intermediate Vector Bosons, W^\pm) (for a review of the theory, see Abe 73, Wei 74). Weak neutral currents were first observed in neutrino-nucleon scattering at CERN (Has 73) and Fermilab (Ben 74) and subsequently in neutrino-electron scattering experiments (Mas 76, Fai 76, Rei 76). The results of all neutrino experiments are by now in excellent agreement with the Weinberg-Salam model (Abb 78). After the initial formulation of the Weinberg-Salam model a large variety of unified gauge models emerged. Some of these models had identical predictions to the Weinberg-Salam model for the neutrino couplings but differed in their expectations for the electron-nucleon couplings.

The electron-nucleon couplings may be determined experimentally by observing parity non-conservation in the electron-nucleon interaction. Parity non-conservation due to weak neutral currents was first observed in polarized electron scattering on deuterium at SLAC (Pre 78) and subsequently in heavy atoms (Bar 79, Con 79a). These results as well as the results presented here strongly support the model of Weinberg-Salam.

Just as the electromagnetic electron-nucleon interaction is mediated by the exchange of virtual photons, the weak electron-nucleon interaction is mediated to first order by the exchange of a virtual Z_0 (see Fig. I.1).

We express the total transition amplitude then as the sum of the electromagnetic and weak contributions:

$$A = A_{em} + A_W \quad (I-1)$$

Transition rates, proportional to A^2 , will then contain interference terms provided the weak and electromagnetic amplitudes are relatively real

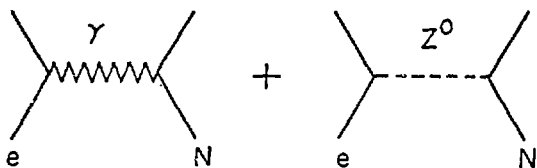
$$A^2 = A_{em}^2 + 2A_{em} A_W \quad (I-2)$$

Where we have assumed $A_W \ll A_{em}$.

The weak amplitude possesses a pseudoscalar part if parity is not conserved. If one designs an experiment to observe a difference in rates between two coordinate systems of opposite handedness (\pm), one then finds asymmetries of the order

$$\Delta = \frac{\sigma_{+}^{-\sigma} - \sigma_{-}^{+\sigma}}{\sigma_{+}^{+\sigma} + \sigma_{-}^{-\sigma}} \sim \frac{A_W}{A_{em}} \approx \frac{G_F}{4\pi\alpha_F/q^2} \quad (I-3)$$

where $G_F = 1.02 \times 10^{-5} m_p^{-2}$, α_F = fine structure constant; and q = momentum transfer. In the SLAC polarized electron experiment, operating at $q^2 \sim (1\text{GeV})^2$ one then estimates an asymmetry



XBL 80I-4572

Figure I-1 Neutral electron-Nucleon amplitudes.

$$\Delta \approx 10^{-4}$$

This is close to the value obtained by a more rigorous treatment. In an atom where $q^2 \approx (m_e \alpha)^2$ one expects typical asymmetries to be of the order of

$$\Delta \approx 10^{-14}$$

When Zeldovitch (Zel 59) first suggested searches for atomic parity non-conservation he realized the impossibility of observing such a small asymmetry. Various methods may be employed to enhance the size of the interference in atoms. First, A_{em} may be reduced by working on an M1 or forbidden transition. A_w may be enhanced either by utilizing a near degeneracy of states of opposite nominal parity (eg. the 2s and 2P levels in Hydrogen) or by using a heavy atom (Bou 74a, 74b, 75) where one obtains a Z^3 enhancement (see Sect. IC). Using such techniques the expected asymmetry increases substantially (see Tables of Section VI). It thus is possible to test the electron-nucleon couplings at momentum transfers differing by five orders of magnitude.

B. Parity Non-Conservation in Atoms

Assuming no derivative couplings, the parity nonconserving neutral current interactions between electrons and nucleons may be described as

$$\mathcal{H}_p = \sum_{k=V,A,S,P,T} C_k G_F (\bar{\psi}_n \Gamma_k \psi_n) (\bar{\psi}_e \Gamma_k \gamma_5 \psi_e) \quad (I-4)$$

where k includes the vector, axial vector, scalar, pseudoscalar, and tensor combinations of Dirac matrices. The pseudoscalar term vanishes in the limit of non-relativistic nucleons. The terms involving S and T are time-reversal-odd and must be at least three orders of magnitude less than the Fermi Constant based on current limits on the permanent electric dipole moments of Xe, Cs, and Tl (Hin 76, Pla 70, Bou 75, Gou 70). We assume then that the weak Hamiltonian possesses only two pseudo-scalar contributions corresponding to $A_e V_n$ and $V_e A_n$:

$$\begin{aligned} \mathcal{H}_p^{(1)} &= \frac{G}{\sqrt{2}} \sum_i \bar{\psi}_e \gamma_\lambda \gamma_5 \psi_e [C_{1p} \bar{\psi}_{pi} \gamma^\lambda \psi_{pi} + C_{1n} \bar{\psi}_{ni} \gamma^\lambda \psi_{ni}] \\ \mathcal{H}_p^{(2)} &= \frac{G}{\sqrt{2}} \sum_i \bar{\psi}_e \gamma_\lambda \psi_e [C_{2p} \bar{\psi}_{pi} \gamma^\lambda \psi_{pi} + C_{2n} \bar{\psi}_{ni} \gamma^\lambda \gamma_5 \psi_{ni}] \end{aligned}$$

where we sum over all protons (p) and neutrons (n). The Weinberg-Salam Model predicts the coupling constants to be:

$$\begin{aligned} C_{1p} &= \frac{1}{2} (1 - 4 \sin^2 \theta) \\ C_{1n} &= -\frac{1}{2} \\ C_{2p} &= g_A/2 (1 - 4 \sin^2 \theta) \\ C_{2n} &= -g_A/2 (1 - 4 \sin^2 \theta) \end{aligned} \tag{I-5}$$

θ = Weinberg angle and

$g_A = 1.25$ is the Axial vector coupling constant of β decay.

A nonrelativistic reduction of the nucleonic currents results in an effective weak electronic Hamiltonian corresponding to $A_e V_n$

$$\mathcal{H}_W^{(1)} = \frac{G}{2\sqrt{2}} Q_W \rho_N(\vec{r}) \gamma_5 \quad (I-6)$$

where $\rho_N(\vec{r})$ is the nuclear density and

$$Q_W = (1-4\sin^2\theta)Z-N \quad (I-7)$$

is the weak charge and \vec{r} is the position of the electron.

In the additional limit of a nonrelativistic electron and a point nucleus one then obtains the effective potentials

$$V_P^{(1)} = \frac{G}{4\sqrt{2}} Q_W [\vec{\sigma} \cdot \vec{p} \delta^3(\vec{r}) + \delta^3(\vec{r}) \vec{\sigma} \cdot \vec{p}] \quad (I-8)$$

and

$$V_P^{(2)} = \frac{G}{4\sqrt{2}} (1-4\sin^2\theta) g_A \vec{\sigma}_N \cdot \vec{\sigma} [\vec{\sigma} \cdot \vec{p} \delta^3(\vec{r}) + \delta^3(\vec{r}) \vec{\sigma} \cdot \vec{p}] \quad (I-9)$$

where $\vec{\sigma}$ and \vec{p} are the spin and momentum of the electron and $\vec{\sigma}_N$ is the nucleon spin. One notes that $V_P^{(2)}$ scales roughly as Z^2 (one factor of Z for the momentum and one for the value of the wave function at the origin), whereas $V_P^{(1)}$ has an additional factor proportional to Z in Q_W . The additional factor of Z appears because the sum over the nucleons is coherent over an electron de Broglie wavelength, whereas the nuclear spins appearing in $V_P^{(2)}$ cancel in pairs. In addition the factor $(1-4\sin^2\theta) \approx .08$ for $\sin^2\theta \approx .23$ suppresses $V_P^{(2)}$ even further. Consequently, in a heavy atom $V_P^{(1)}$ dominates. In addition, the factor $(1-4\sin^2\theta)$ in C_{1p} implies that the neutrons dominate in $\mathcal{H}_W^{(1)}$. Consequently, current heavy atom experiments are primarily sensitive to C_{1n} . It should be noted that this pseudoscalar

Hamiltonian can only connect states of opposite parity and non-vanishing electron density at the origin (i.e., only $S_{1/2}$ and $P_{1/2}$ states). Also, it has been shown (Bou 74a) that the electron-electron parity violating Hamiltonian is very small by comparison due to the mutual repulsion of the electrons.

C. Parity Non-conservation in T1

The $6P_{1/2} - 7P_{1/2}$ transition in T1 is nominally forbidden M_1 (see Fig. I.2). The weak pseudoscalar Hamiltonian (\mathcal{H}_p) modifies the $6P_{1/2}$ and $7P_{1/2}$ states slightly by admixing various states:

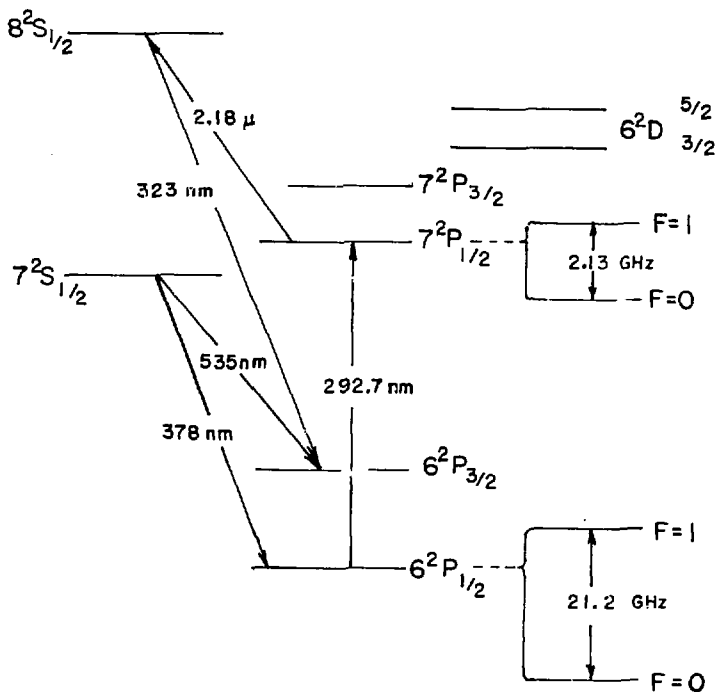
$$\begin{aligned} |\widetilde{6P}_{1/2}\rangle &= |6P_{1/2}\rangle + \sum_n \frac{\langle nS_{1/2} | \mathcal{H}_p | 7P_{1/2} \rangle}{E_{nS} - E_{6P}} |nS_{1/2}\rangle \\ |\widetilde{7P}_{1/2}\rangle &= |7P_{1/2}\rangle + \sum_n \frac{\langle nS_{1/2} | \mathcal{H}_p | 7P_{1/2} \rangle}{E_{nS} - E_{7P}} |nS_{1/2}\rangle \end{aligned} \quad (I-10)$$

where $E_{6P} = 6^2 P_{1/2}$ energy, etc.

Since the states are no longer exact eigenstates of parity, allowed E1 transitions may occur, resulting in an additional parity non-conserving electric dipole amplitude:

$$\epsilon_p = \sum_{nS} \frac{\langle 7P_{1/2} | E1 | nS \rangle \langle nS | \mathcal{H}_p | 6P_{1/2} \rangle}{E_{6P} - E_{nS}} + \frac{\langle 7P_{1/2} | \mathcal{H}_p | nS \rangle \langle nS | E1 | 6P_{1/2} \rangle}{E_{7P} - E_{nS}} \quad (I-11)$$

This yields a total absorption cross section $\sigma_{\pm} = |\epsilon_p \mp iM|^2$ for \pm photon helicities. It can be shown from time reversal invariance (Bou 74b) that ϵ_p and M are relatively imaginary.



XBL 811-7635

Figure I.2 Level structure of Thallium (not to scale).

This then implies a circular dichroism in the transition

$$\delta = \frac{\sigma_+ - \sigma_-}{\sigma_+ + \sigma_-} = \frac{2\text{Im}\epsilon_p}{M} \quad (1-12)$$

since $\epsilon_p \ll M$.

Our goal is to predict and measure δ to sufficient precision to place some meaningful restrictions on the couplings predicted by the Weinberg-Salam model.

II. SEMI-EMPIRICAL DETERMINATION OF δ

A. General Description

In order to obtain a theoretical expression for δ it is necessary to know M and ϵ_p .

M is known from an interference experiment (Chu 77) which utilizes an external electric field E . One measures $-\frac{2M}{\beta E}$, $\frac{4M}{3\alpha E}$, in the absorption $6^2P_{1/2} \rightarrow 7^2P_{1/2}$. Here β is the Stark amplitude for linear polarization of absorbed radiation perpendicular to the applied electric field, given by:

$$\beta = \frac{e^2}{9} \sum_{nS} R_{7P,nS} R_{nS,6P} \left(\frac{1}{E_{6P} - E_{nS}} - \frac{1}{E_{7P} - E_{nS}} \right) + \frac{e^2}{9} \sum_{nD_{3/2}} R_{7P,nD_{3/2}} R_{nD_{3/2},6P} \left(\frac{1}{E_{7P} - E_{nD_{3/2}}} - \frac{1}{E_{6P} - E_{nD_{3/2}}} \right) \quad (\text{II-1})$$

where $R_{7P,nS} = \langle 7^2P_{1/2} | \vec{r} | n^2S_{1/2} \rangle$, etc., and \vec{r} is the electron radial coordinate. Also α is the Stark amplitude for linear polarization parallel to the electric field:

$$\alpha = \frac{e^2}{9} \sum_{nS} R_{7P,nS} R_{nS,6P} \left(\frac{1}{E_{6P} - E_{nS}} - \frac{1}{E_{7P} - E_{nS}} \right) + \frac{2e^2}{9} \sum_{nD_{3/2}} R_{7P,nD_{3/2}} R_{nD_{3/2},6P} \left(\frac{1}{E_{7P} - E_{nD_{3/2}}} + \frac{1}{E_{6P} - E_{nD_{3/2}}} \right) \quad (\text{II-2})$$

Since α, β have never been measured directly, the determination of M depends on a reliable calculation of these quantities.

Theoretical determination of the parity violating amplitude ϵ_p (eq. I.11) also requires evaluation of an infinite sum involving similar radial matrix elements. The pseudoscalar terms $\langle nS | \hat{\epsilon} \cdot \vec{r} | n'P \rangle$ depend on the electron wave functions and their derivatives at the origin. They have been calculated using eq. (I-6) in a one-electron in a central field approximation by various authors (Neu 77, Khr 76). The electric dipole terms of the sum may be expressed as:

$$\langle nS_{1/2} | E1 | n'P_{1/2} \rangle = e \langle nS | \hat{\epsilon} \cdot \vec{r} | n'P_{1/2} \rangle = \frac{e}{3} R_{nS, n'P}$$

where $\hat{\epsilon}$ is the photon polarization vector. It is clear that accurate values of the radial matrix elements $R_{nS, n'P}$ and $R_{nD_{3/2}, n'P}$ would improve the theoretical estimate of δ , α , and β .

The A coefficient between a $P_{1/2}$ state and either a $D_{3/2}$ or $S_{1/2}$ state may be expressed as:

$$A = \frac{4}{9} e^2 R_{n'P, n'S}^2 | E_{nP} - E_{n'S} |^3$$

The $7^2S_{1/2}$ and $6^2D_{3/2}$ states play a dominant role in the sums of eq'ns I-11, II-1, and II-2 (see Table II-6). $A(7S_{1/2} - 6P_{1/2})$ and $A(6D_{3/2} - 6P_{1/2})$ are already known (Gal 64). We here describe measurements of $A(6D_{3/2} - 7P_{1/2})$ and $A(7P_{1/2} - 7S_{1/2})$. Using radial matrix elements implied from these rates, we have improved the theoretical estimate (Neu 77) of δ and have made a realistic assessment of the errors involved. In all of our measurements we employ Tl with the natural isotopic abundance (29.5 percent Tl^{203} and 70.5 percent Tl^{205}).

B. $7P_{1/2}$ Lifetime

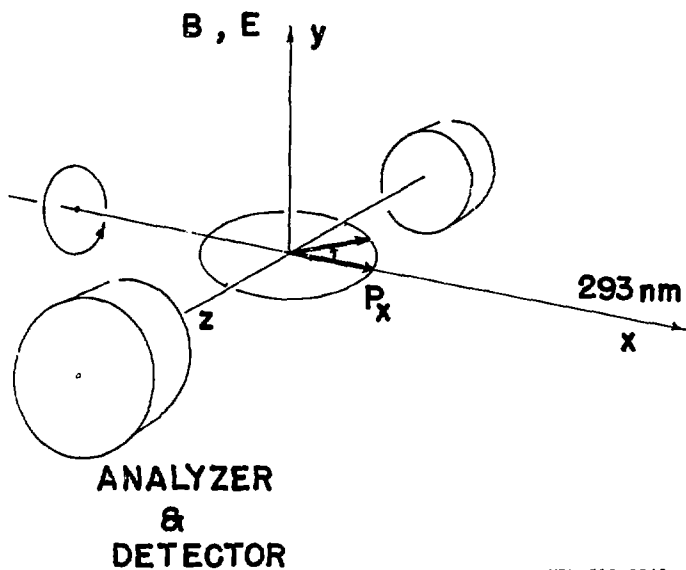
We measure the $7P_{1/2}$ lifetime through observation of the Hanle effect. Circularly polarized laser light tuned to the $6P_{1/2} \rightarrow 7P_{1/2}$ transition at 292.7 nm travels along \hat{x} in thallium vapor, as shown in Fig. II.1. An electric field \vec{E} along \hat{y} induces Stark electric dipole absorption amplitudes αE and βE . When the laser is tuned to the $F = 1 \rightarrow F' = 1$ hyperfine transition, interference between α and β amplitudes causes a polarization along \hat{x} :

$$P_x = \pm \frac{4\alpha\beta}{3\alpha^2 + 2\beta^2} \approx .74 \quad (\text{II-3})$$

where \pm refer to laser photon helicities ± 1 . A weak magnetic field B along y causes P_x to precess in the x - z plane at a rate $\omega = g_F \mu_0 B / \hbar$, where μ_0 is the electron Bohr magneton and g_F is the Lande g factor of the state. Photomultipliers along $\pm z$ detect the left circularly polarized ($h = +1$) component of the $7S_{1/2} - 6P_{3/2}$ decay fluorescence at 535.0 nm. This fluorescence originates from cascade decays $7P_{1/2} \rightarrow 7S_{1/2} \rightarrow 6P_{3/2}$ or from conversion of resonantly trapped 377.6 nm radiation ($7S_{1/2} - 6P_{1/2}$).

The cascade process dilutes the original polarization by a factor of six. An additional factor is lost because of resonance trapping, imperfect polarization analysis, and imperfect initial polarization of the 292.7 nm light.

It may be shown that the observed circular polarization is given by the formula:



XBL 813-8540

Figure II.1 Schematic of experimental arrangement for $7P_{1/2}$ lifetime measurement.

$$\langle P_z \rangle_{535 \text{ nm}} = \frac{b(a + a')}{(1 + a^2)(1 + a'^2)} \quad (\text{II-4})$$

where

$$a' = \frac{eB}{2m_e c A(7S)_{\text{Total}}}, \quad a = \frac{eB}{6m_e A(7P_{1/2})}, \quad \text{and } b = \text{overall}$$

analyzing power. In order to determine $A(7P_{1/2})$ we measure $\langle P_z \rangle$ vs B . The overall scale factor b need not be known to determine $A(7P_{1/2})$. Only the shape of the curve and in particular the position of the maximum is important. From previous measurements (Gal 64)

$$A(7S)_{\text{Total}} = (13.3 \pm 0.3) \times 10^7 \text{ sec}^{-1}. \quad (\text{II-5})$$

The 292.7 nm is generated using the same technique and equipment described in section III.A. Circular polarizations of opposite helicities are produced with a carefully aligned quarter wave plate mounted on a precision one-hundred and eighty degree rotator which flips the quarter wave plate about an axis at 45° to both the fast and slow optic axis.

A sealed off quartz thallium cell was utilized for this measurement. The cell is surrounded by a large stainless steel oven mounted inside a crude vacuum. A separate "stem" heater surrounds a quartz protrusion from the bottom of the cell where the thallium condenses. The stem heater is used to determine the thallium vapor pressure. A chromel-alumel thermocouple is used to measure the stem temperature.

The cell is supported from below by a grounded stainless steel electrode, external to the cell. A pulsed voltage of 600 V is applied

to a second stainless steel electrode which rests on top of the cell, 12.5 mm away from the grounded plate. The Stark polarization (eqn. II-3) is independent of the amplitude of the electric field and hence no precise calibration of the electric field is required.

The magnetic field is produced by a pair of Helmholtz coils with 17 inch diameter. The magnetic field increases linearly with the applied voltage according to

$$B(\text{gauss}) = B_0 + (3.80 \pm .04) V (\text{Volts}) \quad (\text{II-6})$$

and varies by less than .5 percent over the fiducial volume as measured with three calibrated hall probes.

The data were taken at various sequences of magnetic field settings. At each magnetic field setting, four signals, each summed over four hundred laser shots on a gated dual scaler, were stored: S_{1+} , S_{1-} , S_{2+} , and S_{2-} . The subscripts 1 and 2 refer to the fluorescence signals observed in phototubes 1 and 2 (along the $\pm z$ axis in Figure II-1) while the + and - refer to the incident U.V. helicity. The asymmetry P_{Han} , corrected for intensity fluctuations and analyzing power is then calculated:

$$P_{\text{Han}} = \frac{1-z}{1+z}$$

$$\text{where } z = \sqrt{(S_{1+}/S_{1-})/(S_{2+}/S_{2-})}$$

The $P_{\text{Han}}-K$ are then fit to the function II-4 using equations II-5 and II-6. The quantity K allows for a systematic offset in the quantity P_{Han} due to a systematic intensity difference between the various configurations. There are then four parameters: b , B_0 , K , and $A(7P_{1/2})$ which are fit to the data. The results of several fits under various experimental conditions are shown in Table II.1. The low density data is very consistent. The high density data shows a slight decrease in the lifetime of the $7P_{1/2}$ state. The analyzing power (b) also falls off at higher density indicating a depolarization due either to collisions or resonance trapping of the 377.6 nm radiation to the ground state. We therefore include only the low density data (i.e., data with stem temperatures less than 850°K) in our final analysis. Combining this data we find

$$A(7P_{1/2}) = (1.71 \pm .07) \times 10^7 \text{ s}^{-1}$$

where we have included the uncertainty in $A(7S_{1/2})$ and in B as well as the statistical uncertainty.

This may be compared to the theoretical values $A(7P_{1/2}) = 1.88 \times 10^7 \text{ s}^{-1}$ (Neu 77a), and $A(7P_{1/2}) = 1.64 \times 10^7 \text{ s}^{-1}$ (Bar 80).

C. $7P_{3/2}$ Lifetime

A measurement of the $7P_{3/2}$ lifetime was also made using a method similar to that outlined in Section IIB. While the $7P_{3/2}$ lifetime does not enter into the present calculation, its measurement aids in distinguishing the various theoretical models.

Table 11.1

Run No.	N (No. Pts)	(d) Temp (mV)	FIT PARAMETERS					$\sum (x_{\text{exp}} - x_{\text{thry}})^2 / N$ ($\times 10^{-6}$)
			$b(\times 10^{-2})$	B_0	$K(\times 10^{-3})$	$A(7P_{1/2})$	$(\times 10^7 \text{ s}^{-1})$	
1(a)	43	20.8	5.58	-.55	1.0	1.79	14.8	
2	23	22.2	5.30	-.81	3.0	1.72	3.5	
3	21	22.2	5.42	-.71	2.9	1.75	1.7	
4	21	22.2	5.77	-.61	3.4	1.63	6.2	
5	22	22.3	5.70	-.73	2.1	1.69	2.2	
6(b)	23	22.3	5.67	-.71	2.7	1.62	5.1	
7(b)	20	22.2	5.79	-.66	3.0	1.66	5.1	
8	23	25.4	4.79	-.81	2.0	1.85	1.2	
9	20	25.5	4.68	-.75	2.4	1.78	.47	
10	23	25.5	4.74	-.75	2.5	1.83	1.2	
11	20	25.6	4.66	-.76	2.7	1.83	1.3	
12	23	20.0	6.00	-.75	2.4	1.72	7.0	
13	21	20.2	5.80	-.79	2.0	1.83	4.3	
14	26	20.5	5.91	-.69	5.6	1.71	4.2	
15	25	20.2	6.45	-.70	5.3	1.66	2.4	
16	21	20.2	6.71	-.85	5.3	1.61	1.3	
17	23	25.0	5.04	-.66	9.0	1.90	4.3	
18	21	25.0	5.10	-.79	8.4	1.70	5.2	
19(c)	25	25.0	5.21	-.68	8.9	1.75	3.4	
Avg $20.0 \leq T < 20.8$						1.73 \pm .03		
Avg $22.2 \leq T < 22.3$						1.68 \pm 0.2		
Avg $25.0 \leq T < 25.6$						1.80 \pm .03		
Avg $T \leq 22.3$						1.71 \pm .02		
Total Avg						1.74 \pm .02		

(a) This data was taken with only two hundred laser pulses integrated/configuration. All other have four hundred laser pulses/configuration.

(b) This data was taken with the laser defocused.

(c) This data was taken with the electronics reversed on the two phototubes.

(d) The temperature in degrees Kelvin $\approx 293 + 25 \times T(\text{mV})$

Note: The density of the thallium is given approximately by the empirical formula

$$\ln(n) = 54.3 - 19.4 \times 10^3/T \text{ where } T \text{ is in } ^\circ\text{K}$$

Table II.2

Run No.	(a)	(b)	FIT PARAMETERS				$\sum (x_{\text{exp}} - x_{\text{thry}})^2 / N$ ($\times 10^{-5}$)
	N (No. Pts)	Temp (mV)	b	B_0	$A(7P_{1/2})$ ($\times 10^7 S^{-1}$)		
1	55	23.2	.244	-.70	2.46	5.2	
2	29	22.5	.256	-.60	2.37	3.0	
3	27	22.5	.253	-.63	2.43	4.0	
4	29	22.5	.265	-.59	2.25	1.0	
5	27	22.6	.258	-.66	2.32	6.0	
Avg.					2.37 \pm .04		

(a) All data was taken with two hundred laser pulses/configuration.

(b) The temperature in degrees Kelvin $\approx 293 + 25 \times T$ (mV).

Note: The density of thallium is given approximately by the empirical formula:

$$\ln(n) = 54.3 - 19.4 \times 10^3/T \text{ where } T \text{ is in } ^\circ\text{K}.$$

The transition $6P_{1/2}(F=0) \rightarrow 7P_{3/2}(F=2)$ was excited using two circularly polarized photons at 568.8 nm. This procedure produces an initial polarization of the $7P_{3/2}$ state ≈ 1 . Because of the higher rate associated with the two photon transition care must be taken to avoid stimulated emission. Data were taken in the same manner as in the measurement of the $7P_{1/2}$ lifetime. The results were fit to function II-4 with

$$a = \frac{eB}{2m_e A(7P_{3/2})}, \quad K = 0$$

The results of this fit are shown in Table II.2. A fit was also performed with $K \neq 0$ with similar results. Folding in the stated uncertainties in B and $A(7S_{1/2})$, the data may be summarized as:

$$A(7P_{3/2}) = (2.37 \pm .09) \times 10^7 \text{ s}^{-1}$$

which may be compared to the theoretical predictions $A(7P_{3/2}) = 2.37 \times 10^7 \text{ s}^{-1}$ (Neu 77a), and $A(7P_{3/2}) = 2.11 \times 10^7 \text{ s}^{-1}$ (Bar 80).

D. Determination of $A(6D_{3/2} - 7P_{1/2})$

We measure $A(6D_{3/2} - 7P_{1/2})$ by exciting the $6P_{1/2} - 6D_{3/2}$ transition and observing the ratio of the decay fluorescences at 378 nm and 353 nm. The A coefficient may be expressed in terms of this ratio and other better known rates in thallium:

$$A(6D_{3/2} \rightarrow 7P_{1/2}) = \frac{A(6D_{3/2} - 6P_{3/2})A(7S)_{\text{Total}}}{U \times A(7S_{1/2} - 6P_{1/2})} - A(6D_{3/2} - 7P_{3/2}) \quad (\text{II-7})$$

where $U = N_{353\text{nm}}/N_{378\text{nm}}$ is the observed photon number ratio corrected for detector efficiency.

A schematic of the apparatus used in this measurement is shown in Fig. II.2. Light at 558 nm is generated using Coumarin 540 dye (Exiton Corp., 50 mg/l methanol) in a flashlamp pumped pulsed laser (Chu 79). An 80 percent reflecting output coupler is used to minimize shot-to-shot fluctuations. The power output is about 2 mj/pulse at a repetition rate of about 10Hz. The frequency is doubled in an INRAD AD*P crystal maintained at $T = 100^\circ\text{C}$ to produce the 277 nm light. The light is reflected into a sealed off quartz cell containing thallium vapor. The subsequent fluorescence, collimated by two one inch quartz f-1 lenses, is simultaneously observed by a Jarrel-Ash 1/2 meter monochromator with 3.0 mm slits viewed with an RCA 8575 phototube, and an EMI 9780 phototube with a Baird 353 nm interference filter. The broad-band acceptance of the monochromator is chosen to enhance light collection and minimize wavelength setting errors.

The signal sizes are digitized, stored, and analyzed with an on-line LSI-11 computer system. The monochromator is tuned back and forth between 378 nm and 353 nm while the phototube viewing 353 nm is used to normalize the signals. When observing 353 nm an optical attenuator is inserted before the monochromator slit to approximately equalize the observed light intensities between 353 nm and 378 nm. The normalized ratio of the signal in 353 nm with attenuator (Configuration I), to 378 nm without the attenuator (Configuration II), is then measured. Data were taken at thallium vapor densities between

$10^{10} - 10^{11} \text{ cm}^{-3}$. These low densities are chosen to avoid resonance trapping of 277 nm and 378 nm light.

Data taken at a thallium density of 10^{12} cm^{-3} evidence the onset of resonance trapping and hence are not used. The experiment utilizes a focussed detector. High densities attenuate the 378 nm light as it traverses the cell. Most of the atomic excitation then occurs before the viewed interaction region. While no 353 nm fluorescence is viewed from this region, some of the 378 nm light is rescattered and collected. This effect more than compensates for the loss of 378 nm light from the directly viewed interaction region due to resonance trapping. Consequently, we observe U to decrease at higher densities.

The only atomic background observed during this experiment had the following characteristics:

- a) It occurs only when the laser is incident on the cell wall;
- b) The observed fluorescence is enhanced in both 378 nm and 353 nm, however, the fractional increase is greater at 378 nm, producing a reduction in U ; and
- c) It requires the laser to be tuned to the $6P_{1/2} \rightarrow 6D_{3/2}$ resonance.

This signature is consistent with enhanced decay fluorescence due to collisions of excited thallium atoms with the quartz surface. Data are taken at three positions various distances from the cell wall. Agreement in the measured value of U at all three positions (see Table II.3), indicates that this background was not a significant problem in the present measurement.

Table II.3

Position	F(6P _{1/2})	ρ (cm ⁻³)	U
1	1	10 ¹⁰	1.07 ± .01
1	1	10 ¹¹	1.08 ± .01
2	1	10 ¹¹	1.12 ± .01
2	∅	10 ¹¹	1.07 ± .03
3	1	10 ¹¹	1.12 ± .02

Table II.4

Tube Voltage	(C ₃₇₈ /C ₃₅₃)	(C ₃₇₈ /C ₃₅₃) _{W/O}	(C _{378W/O} /C ₃₅₃)
750	2.06	2.02	138
850	2.03	1.97	136
1000	1.99	1.98	137

W/O indicates that this current was measured without the attenuator. All other currents were measured with the optical attenuator in place.

Measurements are also made from each of the two ground state hyperfine components. Since the signal size is substantially larger for the transition from the $6P_{1/2}(F=1)$ Hyperfine Component, any constant background would produce a discrepancy in U when the transition originates in the $(F=1)$ and $(F=0)$ groundstate hyperfine components. No such discrepancy occurs (see Table II.3).

We summarize the data of Table II.3 as

$$S_I/S_{II} = 1.10 \pm .03 \quad (\text{II-8})$$

where S_I and S_{II} are the signals observed in configuration I and II.

Calibration of the relative detection efficiencies of each configuration is accomplished by replacing the thallium cell with an N.B.S. calibrated 1000W Quartz-Iodine lamp. The monochromator phototube current is monitored at the two different frequencies with and without the attenuator. The results are shown in Table II.4. We find no evidence for saturation even at relatively high output currents. The result is

$$C_{II}/C_I = 137 \pm 1 \quad (\text{II-9})$$

where C is the measured output current in each configuration and may be expressed as:

$$C = D \times \int \Delta \lambda \times \frac{\lambda}{hc} \quad (\text{II-10})$$

where we define D to be the detector efficiency of the configuration,

$$\int = \frac{\text{power emitted}}{\text{unit bandwidth}},$$

and for a monochromator $\Delta \lambda = k\lambda$ where $k = \text{constant}$. Thus, the relative detection efficiency of the two configurations is

$$D_{II}/D_I = \frac{C_{II}}{C_I} \frac{\int_{353}}{\int_{378}} \left(\frac{3530}{3776} \right)^2 \quad (\text{II-11})$$

Using the given intensities \int_{353} and \int_{378} of the calibration lamp and equation (II-9):

$$D_{II}/D_I = 70 \pm 2 \quad (\text{II-12})$$

We thus determine the ratio of the emitted photons in the experiment to be

$$U = (1.10 \pm .03) (70 \pm 2) = 77 \pm 4 \quad (\text{II-13})$$

Using Eq'n (II-8), the measured values of A coefficients to $6P_{1/2}$ and $6P_{3/2}$ states, and a theoretical value (Neu 77a) (with much larger fractional uncertainty) for the small A coefficient $A(6D_{3/2} \rightarrow 7P_{3/2})$, one obtains:

$$A(6D_{3/2} \rightarrow 7P_{1/2}) = (5.97 \pm 0.78) \times 10^5 \text{ s}^{-1} \quad (\text{II-14})$$

This may be compared with the theoretical values of $4.79 \times 10^5 \text{ s}^{-1}$ (Neu 77a) and $4.41 \times 10^5 \text{ s}^{-1}$ (Bar 80).

E. Determination of α , β , M , ϵ_p , and δ

In order to make the best estimate of α , β , M , ϵ_p and δ we employ experimental numbers wherever available. Otherwise the results of calculations of Neuffer and Commins (Neu 77a) are used. It is difficult to estimate the contribution of the continuum and autoionizing states when the central-field potential is allowed to vary as a function of orbital angular momentum as is the case for the calculation of Bardsley and Norcross (Bar 80). However, the Green's function technique employed by Neuffer and Commins (Neu 77a) allows one to calculate these contributions in a consistent way.

The A coefficients and radial matrix elements relevant to the calculation are listed in Table II.5. Fifteen percent uncertainties have been assumed for all radial matrix elements which have not been measured. Because of the high accuracy of the calculations of the hyperfine structure of the $6P_{1/2}$ and $7P_{1/2}$ states (which are very sensitive to the values of the wave function near the origin) we have assumed a ten percent uncertainty in the parity violating amplitudes $6P_{1/2} - nS_{1/2}$. However, we have assigned a fifteen percent uncertainty to the parity violating amplitudes $7P_{1/2} - nS_{1/2}$. In addition we have assumed that the contributions to α and β due to continuum and autoionizing $D_{3/2}$ states are overestimated by about thirty percent, as is suggested by the measurements of $6P_{1/2} - nD_{3/2}$

A-coefficients. A fifty percent uncertainty is assigned to these terms. All other continuum and autoionizing sums have been assumed to be valid to thirty percent. The contributions of each intermediate state and its uncertainty in the calculation of α , β , and ϵ_p are shown in Table II.6.

With the above assumptions one obtains the following values of α and β :

$$\alpha = (2.30 \pm .26) \times 10^{-5} \mu_0 \text{cm/V} \quad (\text{II-15})$$

$$\beta = (1.75 \pm .14) \times 10^{-5} \mu_0 \text{cm/V} \quad (\text{II-16})$$

$$\left(\frac{\alpha}{\beta}\right)_{\text{Theo}} = .76 \pm .17 \quad (\text{II-17})$$

where μ_0 is the electron Bohr Magnetron. The theoretical value of (α/β) agrees well with the measured experimental ratio of $.84 \pm .05$ (Chu 77).

The new estimates of α and β change the calibration of the M1 experiment and lead to a new value of M1 amplitude:

$$M_{\text{exp}} = (-2.3 \pm .3) \times 10^{-5} \mu_0 \quad (\text{II-18})$$

The new value of ϵ_p is

$$\epsilon_p = i(1.63 \pm .72) Q_W \times 10^{-10} \mu_0 \quad (\text{II-19})$$

For $\sin^2 \theta = .23$ and $Q_W = (1 - 4\sin^2 \theta)Z - N \approx -117$ one then obtains a new theoretical estimate of δ :

$$\delta_{\text{theo}} = \frac{2\text{Im}\epsilon_p}{M} = (1.7 \pm .8) \times 10^{-3} \quad (\text{II-20})$$

Table II.5

	$A_{\text{CALC}}^{(\text{Neu } 77a)}$ ($\times 10^7 \text{ s}^{-1}$)	A_{exp} ($\times 10^7 \text{ sec}^{-1}$)	$R_{\text{CALC}}^{(\text{Neu } 77a)}$	R_{exp}^*	fractional uncertainty in R
$6P_{1/2} \rightarrow 7S_{1/2}$	5.78	$6.25 \pm .31$	294.1	305.8	.025
8	1.75	$1.78 \pm .16$	91.5	92.3	.045
9	.777	$.78 \pm .10$	51.8	51.9	.064
10	.412	-----	35.1	-----	.15
11	.244	$.31 \pm .06$	26.0	29.3	.097
$7P_{1/2} \rightarrow 7S_{1/2}$	1.88	$1.71 \pm .07$	-1072.6	-1023.	.021
8	.338	-----	991.6	-----	.15
9	.127	-----	219.5	-----	.15
10	.064	-----	114.3	-----	.15
11	.038	-----	75.1	-----	.15
$6P_{1/2} \rightarrow 6D_{3/2}$	16.04	12.60 ± 1.0	-307.7	-272.7	.040
7	6.39	4.40 ± 0.5	-154.8	-128.5	.067
8	3.19	1.89 ± 0.3	-99.8	-76.8	.079
9	1.82	$.98 \pm 0.22$	-71.9	-52.8	.112
10	1.14	$.58 \pm 0.15$	-55.2	-39.4	.129
$7P_{1/2} \rightarrow 6D_{3/2}$.0479	$.0597 \pm .0078$	1321.4	1475.2	.065
7	.416	-----	-489.2	-----	.15
8	.270	-----	-254.2	-----	.15
9	.168	-----	-165.8	-----	.15
10	.099	-----	-120.0	-----	.15

* In these columns we employ units ($\hbar = c = m_e = 1$)

Table II.6

Int. State	$\frac{R_{7P,nS} R_{nS,6P}}{E_{6P} - E_{nS}}$ ($\times 10^{11}$)	$\frac{R_{7P,nS} R_{nS,6P}}{E_{7P} - E_{nS}}$ ($\times 10^{11}$)	Int. State	$\frac{R_{7P,nD} R_{nD,6P}}{E_{6P} - E_{nD}}$ ($\times 10^{11}$)	$\frac{R_{7P,nD} R_{nD,6P}}{E_{7P} - E_{nD}}$ ($\times 10^{11}$)
7S _{1/2}	+4.88 ± .016	-1.682 ± .055	6D _{3/2}	+4.78 ± .037	+8.823 ± .673
8S _{1/2}	-.097 ± .015	-.823 ± .129	7D _{3/2}	-.062 ± .010	-.333 ± .053
9S _{1,2}	.011 ± .002	-.052 ± .009	8D _{3/2}	-.018 ± .003	-.077 ± .012
10S _{1/2}	-.004 ± .001	-.015 ± .003	9D _{3/2}	-.008 ± .001	-.030 ± .006
11S _{1,2}	-.002 ± .001	-.007 ± .001	10D _{3/2}	-.004 ± .001	-.015 ± .003
All other S _{1/2}	-.014 ± .004	-.130 ± .043	All other D _{3/2}	-.048 ± .024	-.693 ± .347
TOTAL	+3.60 ± .022 ≡ S ₆	-2.709 ± .147 ≡ S ₇	TOTAL	+3.38 ± .045 ≡ D ₆	+7.675 ± .759 ≡ D ₇

$$B = \frac{e^2}{9} (S_6 - S_7 + D_7 - D_6) = (+1.16 \pm .09) \times 10^{11} e^2$$

$$B = (+1.75 \pm .14) \times 10^{-5} \nu_0 \text{ cm/V}$$

$$\alpha = \frac{e^2}{9} (S_6 + S_7 + 2D_6 + 2D_7) = (+1.52 \pm .17) \times 10^{11} e^2$$

$$\alpha = (2.30 \pm .26) \times 10^{-5} \nu_0 \text{ cm/V}$$

$$\langle 7P_{1/2} | E | nS \rangle \langle nS | H_p | 6P_{1/2} \rangle \quad \langle 7P_{1/2} | H_p | nS \rangle \langle nS | E | 6P_{1/2} \rangle$$

$$\frac{E_{6P} - E_{nS}}{(i \times 10^{-10} Q_W \nu_0)} \quad \frac{E_{7P} - E_{nS}}{(i \times 10^{-10} Q_W \nu_0)}$$

$$6S \quad -20 \pm .03 \quad .63 \pm .13$$

$$7S \quad 4.85 \pm .56 \quad -1.76 \pm .27$$

$$8S \quad -1.77 \pm .38 \quad .49 \pm .08$$

$$9S \quad -.23 \pm .05 \quad .09 \pm .02$$

$$10S \quad -.08 \pm .02 \quad .04 \pm .01$$

$$\text{All other S states} \quad -43 \pm .13$$

$$\text{TOTAL} \quad 1.63 \pm .76$$

$$r_p = i(1.63 \pm .72) \times 10^{-10} Q_W \nu_0$$

Note: All units are ($\hbar = m_e = c = 1$) unless otherwise noted

III. DESCRIPTION OF THE EXPERIMENT

A. Experimental Method and Apparatus

To measure δ we employ a method first suggested by Bouchiat and Bouchiat (Bou 75a), in which an external electric field E is applied to Tl vapor. This field Stark-mixes $^2P_{1/2}$ states with $^2S_{1/2}$ and $^2D_{3/2}$ states. The $6P_{1/2} - 7P_{1/2}$ transition intensity, proportional to E^2 , is thus increased above background (the latter being due to light scattering and atom-atom collisions). Interference between M and the Stark amplitude, and between ϵ_p and the Stark amplitude, results in a polarization of the $7^2P_{1/2}$ state. Let the 293 nm (uv) photon beam be along \hat{x} and choose $\underline{\xi} = E\hat{y}$ (see Fig. III.1a). One then finds the $7^2P_{1/2}$ polarization along z to be:

$$P_z (F = 0 \rightarrow F' = 1) \approx -\frac{2M}{8E} (1 \pm \delta/2) \quad (\text{III-1})$$

$$P_z (F = 1 \rightarrow F' = 1) \approx \frac{(4\alpha - 2\beta)M}{(3\alpha^2 + 2\beta^2)E} (1 \pm \delta/2) \quad (\text{III-2})$$

$$P_z (F = 0 \rightarrow F' = 0) = 0 \quad (\text{III-3})$$

for each indicated hfs component $\delta^2P_{1/2}$, $F \rightarrow 7^2P_{1/2}$, F' of the transition (Flu 76). Here \pm refer to ± 293 nm photon helicities.

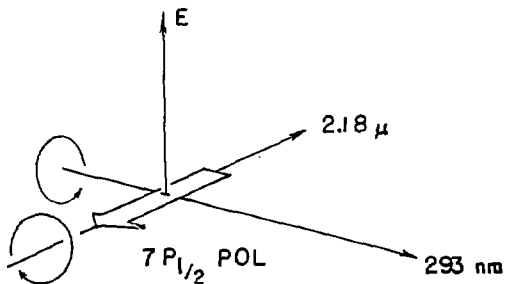
The parity nonconserving terms in the polarization (i.e., those proportional to $\delta/2$ in equations III-1,2) are pseudoscalars of the general form $h \underline{k} \times \underline{\xi} \cdot \underline{L}$ where h is the photon helicity, \underline{k} is the photon wave vector, and \underline{L} is the atomic angular momentum in the $7^2P_{1/2}$ state. Although the pseudoscalar term arises from interference between

ϵ_p and αE and/or βE we express it in terms of δ , since the latter quantity is measured more accurately than either M or ϵ_p separately in the present experiment.

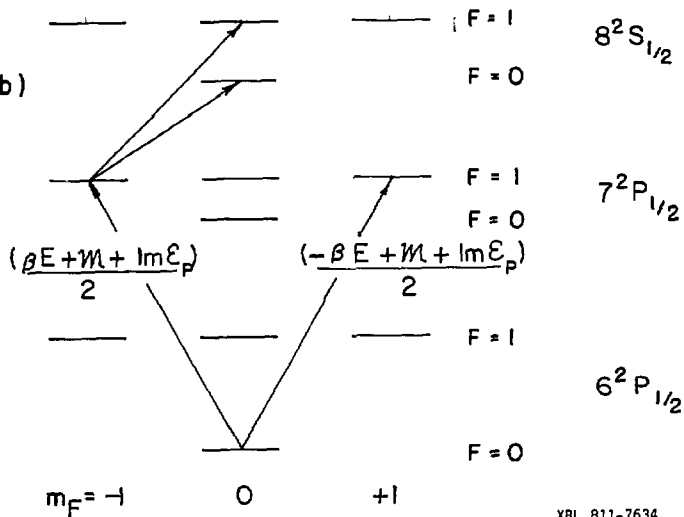
We analyze the $7^2P_{1/2}$ polarization by selective excitation of the $m_F = +1$ or -1 components of this state to the $8^2S_{1/2}$ state, using circularly polarized 2.18μ light, directed along $-z$, and we observe the intensity of 323 nm ($8^2S_{1/2} - 6^2P_{3/2}$) fluorescence (see Fig. III.1b). The polarization analyzing power of this method is approximately 0.7 (Con 79).

Figure III.2 is a schematic diagram of the apparatus, which we now describe in detail. The cell consists of a "main" section which encloses the electric field region, and a "stem" section, and are supported by a pumpout tube which is normally kept closed by means of a remotely actuated ground quartz ball-and-socket valve. Surrounding the cell are the "main" and "stem" ovens, which are electrically heated stainless steel (see Fig. III.3). The cell body consists of a suprasil cylinder (Amersil Corp.) of 69 mm o.d., 2 mm. wall thickness, fused to top and bottom fused quartz end-plates. The cylinder was carefully selected for high optical quality. The electrodes are flat tantalum plates, 1 mm. thickness, suspended from the cell ceiling by quartz rods and spacers. The electrode separation is 14 mm. The connecting tantalum wires pass through closely fitting quartz capillary tubes to tungsten-glass feedthroughs in the cold portion of the cell assembly. Thallium condenses in the capillaries and seals them.

a)

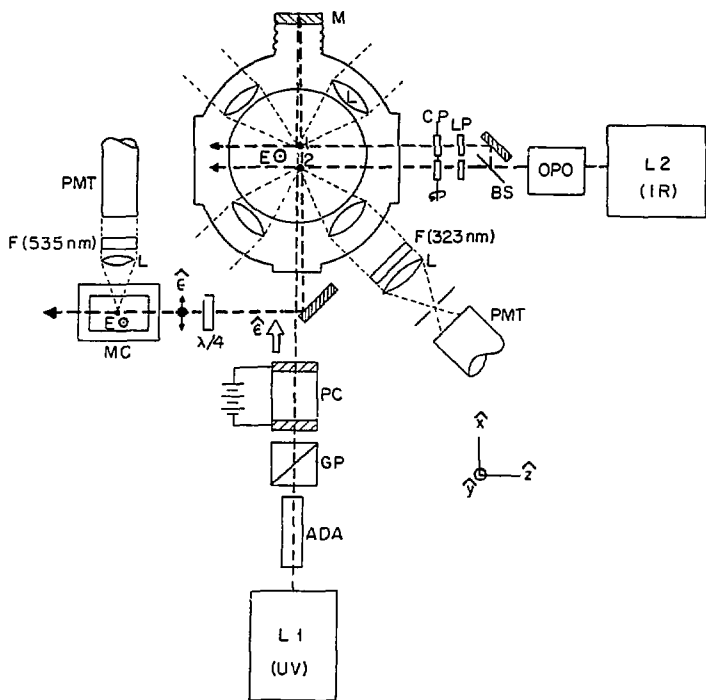


b)



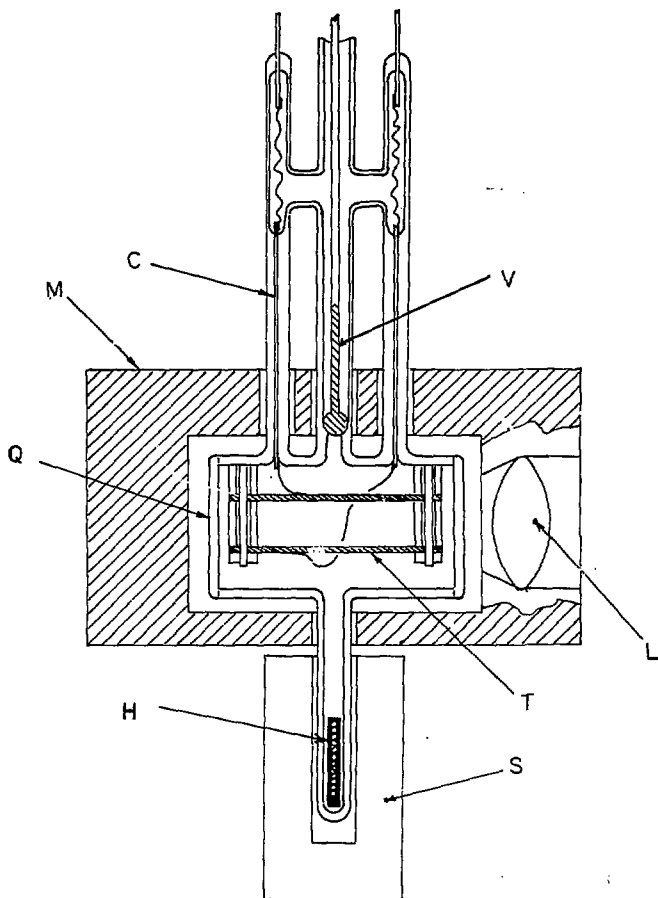
XBL 811-7634

Figure III.1 a) Orientation of electric field polarization, wave vectors in the parity experiment. b) Schematic diagram of energy levels (not to scale), illustrating production of polarization in the $7^2 P_{1/2}$ state, $F=0 \rightarrow F=1$ transition, and analysis of polarization by selective excitation to the $8^2 S_{1/2}$ state. The amplitudes for the transitions $5^2 P_{1/2}$, $F=0$, $m_F=0 \rightarrow 7^2 P_{1/2}$, $F=1$, $m_F=\pm 1$ are shown.



XBL 808-5751

Figure III.2 Schematic diagram of apparatus. L1, L2) Flashlamp pumped pulsed dye lasers; ADA) Doubling crystal; GP) Glan-air polarizing prism; PC) Pockels cell for production of circularly polarized 292 nm light; OPO) Optical parametric oscillator for production of 2.18 μ light; BS) beam splitter; LP) linear polarizers for 2.18 μ light; CP) circular polarizers; E) electric field; L) fused-quartz lenses; LF) liquid filter; F) interference filters; M) retroreflecting mirror; MC) monitor cell.



XBL 811-7633

Figure III.3 Cell and ovens. V) quartz ball valve and lifter; C) capillary tubes; M) main oven; Q) cylindrical cell wall; T) tantalum electrodes; L) lens; S) stem oven; H) tantalum crucible with thallium load.

The stem is a 5 mm o.d. quartz tube below the main body of the cell. It contains a tantalum crucible which is loaded with 99.999 per cent pure thallium metal with the natural isotopic abundances. During the experiment the stem temperature is maintained at about 920°K (corresponding to a Tl vapor density $n = 10^{15} \text{ cm}^{-3}$) and the main portion of the cell is at about 1000°K. The cell-oven assembly is surrounded by three concentric cylindrical stainless-steel heat shields and mounted inside a rough vacuum tank. The pressure in the latter is deliberately maintained at about 5×10^{-3} torr with a controlled air leak so that oven surfaces remain oxidized. This minimizes the presence of chromium and/or manganese vapor which attacks quartz at 1000°K.

The experiment employs two essentially identical flash-lamp pumped tunable pulsed dye lasers (L1, L2), built in this laboratory. Details of design and construction have been reported elsewhere (Chu 79). L1 operates at 585 nm and is used to produce 293 nm light in a doubling crystal for the $6^2P_{1/2} - 7^2P_{1/2}$ transition. The frequency is actively stabilized by computer control of intracavity optics. Typical output energy is 10-12 mj/pulse at a repetition rate of 20 s^{-1} . Laser L-2 delivers 6-7 mj/pulse with a bandwidth of approximately 15 GHz. The two lasers are synchronized and have a relative time jitter of less than 5 ns.

Light from L1 is focussed with an $f = 62 \text{ cm}$ lens into a .5 cm x 5 cm x 5 cm crystal of $\text{NH}_4\text{H}_2\text{A}_8\text{O}_4$ (ADA) for second harmonic generation. The crystal is temperature stabilized to maintain a 90° phase

match condition. Typically we generate 0.6 - 0.7 mj/pulse at 293 nm. Light emerging from the ADA crystal is linearly polarized vertically, orthogonal to the 585 nm pump beam. A Glan-air calcite prism is used to separate the beams and define the uv linear polarization precisely before the beam enters the circular polarizer. The latter is a Pockels cell (Inrad) consisting of a 2 cm crystal of KD^*P (KD_2PO_4) aligned with its principal axis along the beam direction. Application of about ± 1000 V to the Pockels cell's electrodes results in $\pm \lambda/4$ retardation. The voltage is pulsed to eliminate the effects of long term relaxation in the retardation which occurs with a dc electric field, and a slow (100 μs) rise time is chosen to avoid crystal resonances. Initial alignment of the Pockels cell is made optically and final alignment makes use of the Stark effect in thallium itself (see Sec. IVC). The sign of helicity of the uv beam as a function of Pockels cell polarity has been determined optically and by observation of the α - β interference in thallium (see Eq. II-3).

The 2.18 μ light is produced by a Chromatix CMX-4/IR Optical Parametric Oscillator (OPO) driven by L2. The resonant wave in the OPO has $\lambda = 800$ nm, and the difference wavelength is 2.18 μ with a bandwidth of 2 cm^{-1} (Chromatix specification) and a spectral profile with the same mode spacing as the pump (150 MHz). This is sufficient to saturate the $7^2P_{1/2} - 8^2S_{1/2}$ transition, which has a Doppler width of 230 MHz. Typically we obtain .2 - .3 mj/pulse, which is attenuated by 50 percent before entering the cell to maximize analyzing power. Frequency jitter causes 10-15 percent signal fluctuations per

pulse. The 2.18 μ beam is split into two beams of equal intensity with a thin wafer of polished silicon. The two beams pass through individually adjustable linear polarizers (Polaroid HR plastic) and crystalline quartz quarter-wave plates (Virgo Optics) set to produce beams of opposite helicity in the two interaction regions defined by intersection with the uv beam (see Fig. III.2). The fractional difference between signals observed in these two regions is proportional to the polarization P_z and is quite independent of pulse-to-pulse intensity fluctuations of the light beams. The quarter wave plates are rotated automatically about their axis parallel to x once every 128 pulses to reverse the helicity in each region. The 2.18 μ beams are aligned perpendicular to the 293 nm beam to within 1°. A computer controlled solenoid-actuated flag automatically blocks the 2.18 μ beam for background measurements.

The adjustable linear polarizers compensate for imperfections in the orientation of the quarter wave plates. We monitor the signal size asymmetry

$$\Gamma_{ir}^{1,2} = \frac{S_{1,2}(ir+) - S_{1,2}(ir-)}{S_{1,2}(ir+) + S_{1,2}(ir-)}$$

where $ir\pm$ refers to the helicity of the infrared light, and 1,2 refer to regions. By adjusting the rotational orientation of the linear polarizers Γ_{ir}^1 and Γ_{ir}^2 can be made equal and both $\leq 10^{-3}$.

Because the 7P-8S transition is heavily saturated, the asymmetry in the admixture of incorrect polarization when $\Gamma_{ir} = 10^{-3}$ is only

$\sim 2 \times 10^{-5}$. This equalizes the analyzing power for ir^+ and ir^- in each region (although the analyzing power is different in the two regions). By direct measurement, the intensity ratio is:

$$\frac{I(\text{desired helicity})}{I(\text{unwanted helicity})} = \begin{array}{l} .001 \text{ in region 1.} \\ .0025 \text{ in region 2.} \end{array}$$

The rough vacuum tank contains an off-axis rotating window in the front, through which the 293 nm beam enters. This is rotated from time to time by hand so that the uv beam enters through a clean portion of the window. The dielectric mirror at the rear of the tank is used to reflect the uv beam back through the cell. It is back-surfaced so that contaminants from the oven cannot damage the dielectric film. The mirror is mounted off-axis on a rotating seal to allow selection of locations on the mirror which are clean and have minimal birefringence. The reflected beam can be blocked automatically by a solenoid-actuated flag controlled by the computer.

Water cooled magnetic field coils capable of producing ± 8 gauss along the x (uv beam) direction are mounted inside the vacuum tank. These are used for diagnostic purposes (see Sec. IVE). Large diameter coils outside the vacuum system are used to cancel the earth's field and to generate a large magnetic field in the y direction for observation of the Hanle effect (see Sec. IIB).

Each interaction region is viewed by two photomultiplier tubes. The 323 nm fluorescence accompanying $8S_{1/2} - 6P_{3/2}$ decay is collimated by 38 mm dia f/1 fused silica lenses inside the oven, passes through holes in the heat shields and then through double quartz

windows in the detector ports. These windows are cooled by a flowing filtered solution of Phthalic acid (6 g potassium acid phthalate per liter distilled H_2O). This solution is a liquid filter with a sharp low-pass cutoff at about 310 nm (Kas 48). Next in line is an interference filter at 323 nm (peak transmission 25-30 percent, fwhm 2.5 nm) which also contains a UG-11 infrared and visible blocking filter. Finally there is a spatial filter consisting of a 38 mm dia. f/1 quartz lens and an aperture at the focus.

The photomultipliers are 9780 QB (EMI) with alkali photocathodes and quartz windows. The anodes of the two tubes viewing each region are connected together and capacitively coupled to charge integrating preamplifiers. The output pulse is amplified, digitized and sent to an LSI-11/2 computer.

No component introduces electronic or digitizing noise greater than 10^{-3} of the signal, per pulse. A typical signal at each photomultiplier cathode on the 0-1 resonance at a Stark field of 215 V/cm is 10^4 photoelectrons per pulse. The signal-to-background ratio for these conditions is about 10:1. Most of the background is due to scattering and fluorescence of 293 nm laser photons in the cell walls. The remainder arises from atom-atom collisions and miscellaneous small effects.

For linearly polarized uv light with polarization ϵ , only the $F = 0 - F' = 0$ transition is allowed for $\hat{\epsilon} \parallel \underline{E}$, while for $\hat{\epsilon} \perp \underline{E}$, only the 0-1 transition can occur. This fact is used to monitor the frequency of the light. (Here we ignore the 1-1, 1-0 transitions which are

separated from the 0-0,0-1 transitions by about 21 GHz.) After the uv laser beam is reflected back through the main cell and rough vacuum tank, it suffers two 90° reflections from aluminum mirrors with orthogonal planes of incidence. The retardation effects of each reflection cancel, leaving the beam circularly polarized but travelling parallel to -z (see Fig. III-2). It then passes through a fixed quarter wave plate which changes the \pm helicity photons into alternative ϵ_x or ϵ_y linear polarizations. The beam enters a second vacuum tank which houses a separate oven and thallium cell with external electrodes. The fluorescence ($7^2P_{1/2} \Rightarrow 7^2S_{1/2} \Rightarrow 6^2P_{3/2}$) at 535 nm from this cell is viewed by a single phototube. Observation of the signal asymmetry between $I(\epsilon_x)$ and $I(\epsilon_y)$ determines the frequency directly in terms of the ratio $I(0-1)/(0-0)$. This ratio, corrected for background dilution, is averaged over 256 pulses by the computer, which uses the result to tune L1. An intensity ratio $I(0-1)/I(0-0) = 15$ is maintained in the monitor cell, which corresponds to the ratio $I(0-1)/I(0-0) = 11$ in the main cell. The discrepancy is caused by higher efficiency for pumping $F = 0$, $m_F = 0$ $7^2P_{1/2}$ atoms to the $8^2S_{1/2}$ state, than for $F = 1$, $m_F = \pm 1$ atoms.

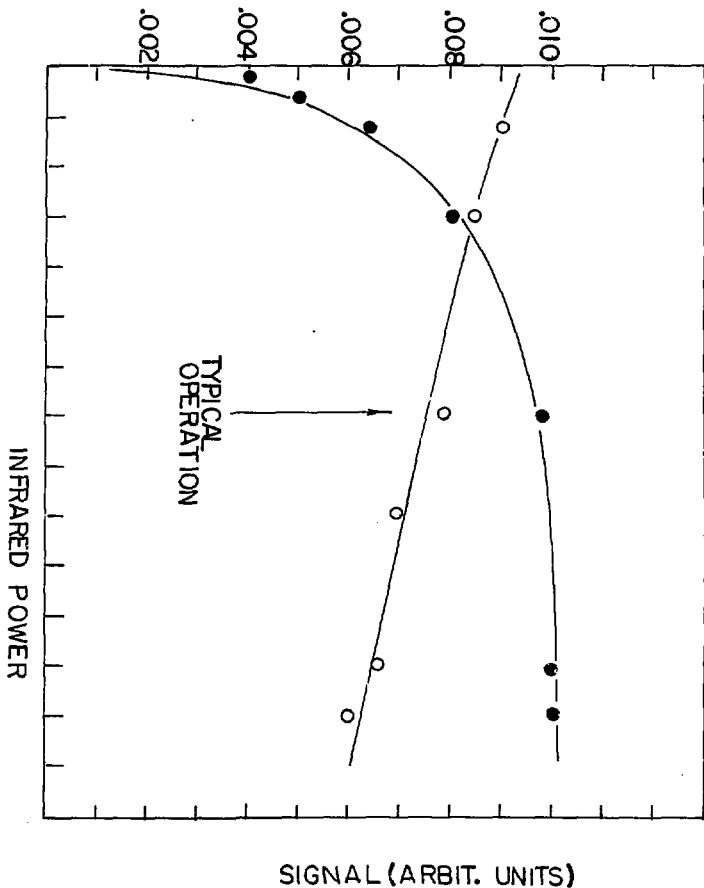
B. Selective Excitation and Analyzing Power

The selective excitation of $7^2P_{1/2}$ atoms to the $8^2S_{1/2}$ state by 2.18 μ circularly polarized light may be calculated in a straightforward way using coupled rate equations for the 8 Zeeman levels (Buc 80). The solution yields the signal size in the 323 nm channel, compared to the 535 nm signal which would be observed if all

$7^2P_{1/2}$ atoms were allowed to decay via 7S. When laser L1 is tuned to the 0-1 transition, 6 percent of the atoms excited to $7^2P_{1/2}$ decay at 323 nm, while on the 0-0 transition, the fraction is 10 percent. The calculations also yield the polarization analyzing power at the frequencies where data are taken, vs. 2.18 μ light intensity, and as a function of purity of 2.18 μ circular polarization. The effects of these can be seen in Fig. III-4. As the infrared intensity increases, the 323 nm signal saturates. Further increase eventually causes a dilution in the measured polarization, due to imperfect 2.18 μ photon helicity.

The analyzing power has been measured by observing an interference between α and β Stark amplitudes in the 1-1 line (see Eqn. II-3). We have performed an experiment in which the 2.18 μ circularly polarized beam propagates along $-x$, opposite to the 293 nm beam. The 323 nm fluorescence exhibits a very large asymmetry depending on uv and ir helicities, arising from $P_x(1-1)$. Observations of this asymmetry yield a measured analyzing power of about 70 percent, in agreement with calculations of selective excitation.

OBSERVED MI ASYMMETRY



XBL 811-7636

Figure III.4 ●: 323 nm fluorescent signal vs. 2.18 μ intensity (right hand scale).

○: Observed MI asymmetry vs. 2.18 μ intensity (left hand scale).

IV. ANALYSIS OF SYSTEMATIC ERRORS AND CORRECTIONS

A. General Remarks

Certain important features of the apparatus and experimental procedure are utilized to reduce or eliminate possible systematic errors. These are as follows:

- a) All parity data are taken on the ($6^2P_{1/2}$, $F = 0 - 7^2P_{1/2}$, $F' = 1$) transition (0-1 line). The polarization for the 0-1 line is about 4.5 times greater than for the 1-1 line (although the total signal is about 7 times less). More important, the 0-1 line is much less susceptible to possible systematic errors than the 1-1 line.
- b) Two interaction regions, with opposite i.r. circular polarizations, are used (as described in Sec. III).
- c) The electric field polarity is reversed with each pulse.
- d) The sign of uv helicity, determined by Pockels cell voltage polarity, is given by the sequence:

+ + + - - - + + - - - + + + - - - . . .

The sequence begins in a random place after each set of 128 pulses. It is chosen to eliminate correlations between E polarity and uv helicity.

- e) The i.r. circular polarization reverses after 128 pulses.
- f) The $7^2P_{1/2}$ polarization consists of a parity nonconserving part $\pm 2 \text{ Im } \epsilon_p / \beta E$ and a parity conserving part $- 2M / \beta E$. The

latter reverses with direction of uv beam and is largely cancelled when the mirror is used. Data are taken with the mirror blocked, and with it unblocked. Background measurements (in which no i.r. reaches the interaction regions but other conditions are the same as for signal) also are taken with and without the mirror. Observations of the parity asymmetry are also carried out on the 0-0 line, as a null experiment.

As will be discussed in detail in Secs. IVC-IVD the remaining sources of possible systematic error not eliminated by these precautions are (1) imperfect uv circular polarization, (2) misaligned electric fields which do not reverse exactly in proportion to the main component of electric field, and (3) magnetic fields. It will be shown that these effects can be measured precisely by a combination of auxiliary experiments, and corrections applied with very small uncertainty.

B. Data Collection

Three digitized signals are received from the computer on each pulse: one from each of the interaction regions (T_1, T_2) and one from the monitor cell. We have $T_{1,2} = S_{1,2} + B_{1,2}$ where S, B denote signal and background, respectively. The T_1, T_2 are compiled into 16 sums denoted by the array T_{ijkl} . Subscripts $ijkl$ are given by the following table:

| | |
|-----------|---------------|
| $i = 0,1$ | uv pol \neq |
| $j = 0,1$ | E \neq |
| $k = 0,1$ | ir pol \neq |
| $l = 1,2$ | Region 1,2 |

After 256 pulses the $T_{ijk\ell}$ are stored on disk. Eight polarizations P are computed by subtracting the regions:

$$P_{ijk} = \frac{T_{ijk1} - T_{ijk2}}{T_{ijk1} + T_{ijk2}} \quad (\text{IV-1})$$

The following quantities are formed:

$$\Delta_M = \frac{1}{8} [(P_{000} - P_{001} - P_{010} + P_{011}) + (P_{100} - P_{101} - P_{110} + P_{111})] \quad (\text{IV-2})$$

$$\Delta_P = \frac{1}{8} [(P_{000} - P_{001} - P_{010} + P_{011}) - (P_{100} - P_{101} - P_{110} + P_{111})] \quad (\text{IV-3})$$

$$\Delta_E = \frac{1}{8} [P_{000} - P_{001} + P_{010} - P_{011}) - (P_{100} - P_{101} - P_{110} + P_{111})] \quad (\text{IV-4})$$

Apart from background and residual systematic effects, to be discussed below, Δ_M is the polarization due to M1-Stark interference: $-2M/\beta E$,

and Δ_p is the parity nonconserving polarization: $-2 \operatorname{Im}(\epsilon_p)/\beta E$. Δ_E and other signals and asymmetries calculated from the $T_{ijk\ell}$ are used for diagnostic purposes and corrections to the data. The data collection sequence is discussed further in sec. VA.

C. The Effects of Imperfect uv Circular Polarization

Various dilutions of the M1-Stark polarization occur because of background, small admixture of 0-0 intensity in the 0-1 line, and imperfection of the 2.18 μ polarization. In addition the M-1 Stark interference depends on \underline{k} and is thus reduced by reflections. If any of these dilutions vary as a function of uv circular polarization, this results in a uv polarization-dependent observed M1 asymmetry which would be interpreted as a (false) parity asymmetry. However, the net effect can be expressed in terms of experimentally measured parameters.

The measured M1 asymmetry may be written:

$$\Delta_M = D_{i,r.} \frac{S_f - S_r}{(S + B)} \Delta_{M0} \quad (\text{IV-5})$$

where Δ_{M0} is the undiluted M1 asymmetry, $D_{i,r.}$ is the i.r. analyzing power, and S_f, S_r are the signals in the 0-1 line for the forward and reflected uv beam, respectively. $D_{i,r.}$ cancels in the ratio Δ_p/Δ_M so we ignore it in the following.

For data taken with the mirror blocked, it can then be shown that (IV-5) becomes:

$$\Delta_M = \frac{S_b}{(S+B)_b} \frac{1}{(f+1)} \frac{1-r}{1+r} \Delta_{MO} \quad (IV-6)$$

where $f = S_{00}/S_{01} = 0.09$, r is the effective reflectance of the quartz cell, and b stands for "blocked data." The false parity asymmetry is then:

$$\Delta_F = \frac{\Delta_{M+} - \Delta_{M-}}{2} \quad (IV-7)$$

where we employ $\Delta_{M\pm}$ for \pm uv circular polarization. It can be shown that (IV-7) becomes:

$$\Delta_F^b = \Delta_{Mb} \left(\frac{1+f}{1-f} \right) \left[\frac{B_b}{S_b} (\Gamma_b - \gamma_b) + \frac{2f}{1+f} \Gamma_b \right] \quad (IV-8)$$

where

$$\Gamma_b = \frac{(S+B)_{b+} - (S+B)_{b-}}{(S+B)_{b+} + (S+B)_{b-}}$$

and

$$\gamma_b = \frac{B_{b+} - B_{b-}}{B_{b+} + B_{b-}}$$

The first term is due to asymmetric background dilutions, the second to 0-0 contamination. Each of the quantities on the RHS of (IV-8) is measured during data collection. Fine adjustment of the Pockel cell

voltage is made during data collection to minimize Γ_b which is nonzero primarily because of polarization imperfections.

Most of our data were collected with the mirror unblocked. This was done to increase signal and reduce systematic effects associated with Δ_M (the latter is decreased by about a factor of 4 when the mirror is unblocked). However, the uv polarization does suffer a slight degradation on reflection from the mirror, which is back-surfaced, and this can also result in a difference $S_f - S_r$ which depends on uv circular polarization. It can be shown that in the "unblocked" case:

$$\Delta_{Fu} = \Delta_{Mb} \left(\frac{1+f}{1-f} \right) \frac{(S+B)_b}{S_b(S+B)_u} \left(2(S+B)_b(\Gamma_b - \Gamma_u) + 2B_b(\Gamma_u - \gamma_b) + B_u(\gamma_u - \Gamma_u) + \frac{2f}{1+f} (2S_b - S_u)\gamma_u \right) \quad (IV-9)$$

The subscript u refers to "unblocked." The first term of the RHS of (IV-9) accounts for forward and reverse beam polarization asymmetries. The other terms describe the dilutions already discussed; all are expressed in terms of measured quantities. It has been assumed in this discussion that the effective reflectance of the front and rear of the cell are the same.

D. The Effects of Stray Electric and Magnetic Fields and Their Couplings to Polarization Imperfections.

A static electric field of ≈ 215 V/cm exists in each interaction region during each pulse. Ideally the field is along the y axis perpendicular to \hat{k} (along \hat{x}) and \hat{z} (the i.r. beam direction). In

reality \underline{k} defines \hat{x} and the 2.18 μ beam(s) define the $\hat{x} - \hat{z}$ plane. \underline{E} may then have x, y, and z components, and \underline{E}_+ , \underline{E}_- may differ slightly in magnitude and direction. We separate \underline{E} into reversing and nonreversing components:

$$\underline{E}_+ = \underline{E}_0 + \underline{\Delta E} \quad , \quad \underline{E}_- = -\underline{E}_0 + \underline{\Delta E} \quad (\text{IV-10})$$

An analysis involving stray electric fields and the possibility of their creating polarizations with the same signature as the parity was first considered by Bouchiat, Guená, and Pottier (Bou 80). In addition to allowing for imperfections in the electric field one must also consider the presence of small residual magnetic fields that would induce Hanle-rotation (see Sect. IIB) of polarizations which would otherwise not be along the z axis. We include these effects and also allow for arbitrary 293 nm polarization imperfections by writing the \pm polarization states as:

$$\hat{R} = \sqrt{1 - \eta^2} \hat{e}_- + \eta e^{i\phi} \hat{e}_+ \quad (\text{IV-14})$$

$$\hat{L} = \sqrt{1 - \eta'^2} \hat{e}_+ + \eta' e^{i\phi'} \hat{e}_- \quad (\text{IV-12})$$

respectively, where η , ϕ , η' , ϕ' are arbitrary real numbers (but $\eta^2 \ll 1$, $\eta'^2 \ll 1$).

Finally, imperfect resolution of the Hyperfine structure is also allowed. It is then possible to write a general state vector describing the Thallium system with all of its imperfections. From

this state vector one may derive all polarizations, some of which have the same signature as the parity. This procedure has been carried out in complete generality and detail (Buc 80). In the appropriate limits for this experiment and after removing the terms which describe polarization imperfections accounted for in the corrections of eqs. (IV-8) and (IV-9), there remains an additional false parity asymmetry:

$$\begin{aligned} \Delta_{\text{FALSE}} = & \frac{2E_{Ox}\Delta E_z}{E_{Oy}^2} - \frac{2\Delta E_x}{E_{Oy}} \left(\frac{E_{Oz}}{E_{Oy}} - \theta_x \right) + \frac{4E_{Ox}\Delta E_y}{E_{Oy}^2} \left(\frac{E_{Oz}}{E_{Oy}} - \theta_x \right) \\ & - \frac{2M}{E_{Oy}^2} \left(\frac{E_{Oz}}{E_{Oy}} + \theta_x \right) \quad (n \sin \phi + n' \sin \phi') \end{aligned} \quad (\text{IV-13})$$

where θ_x is the Hanle precession angle associated with a magnetic field in the \hat{x} direction. In the above we have also dropped the term due to H.F. mixing.

$$\Delta_{\text{HFM}} = \frac{-2\alpha m}{\beta^2 E_{Oy}} (w_x^6 - w_x^7) \quad (\text{IV-14})$$

where $w_x^n = \frac{g_J \nu_O B_x}{2\hbar \Delta \gamma_n}$, B_x is the magnetic field in the x direction and $\Delta \gamma_n$ is the hyperfine splitting of the $n^2P_{1/2}$ state. This term yields a false parity asymmetry equal to that expected for Δ_p when $|B_x| = 5.5$ gauss. However, during the experiment $|B_x| \leq .01$ g, so the contribution due to this term is very small. It is important to consider this term, however, in an auxiliary diagnostic experiment (Sect. IV-E.3), where the field is about 5 gauss.

The generalized state vector also indicates the existence of another polarization which behaves identically to the parity except that it does not reverse with the electric field. In the same limits as equation (IV-13), one finds this polarization to be:

$$\Delta E = \frac{2E_{0x}}{E_{0y}} \left(\frac{-E_{0x}}{E_{0y}} + \theta_x \right) \quad (\text{IV-15})$$

This polarization is very useful for diagnostic purposes.

E. Methods of Measuring False Parity Effects

We now describe independent measurements of E_{0x} , E_{0z} , ΔE_x , ΔE_z , ΔE_y , and $\eta \sin \phi + \eta' \sin \phi'$.

1. Information in Parity Data

ΔE_y : The total signal for each electric field direction, summed over regions and laser polarization, is $S(E_{\pm}) \propto E_{0y}^2 \pm 2E_{0y}E_y$.

We measure the asymmetry:

$$\gamma_E \equiv \frac{S(E_+) - S(E_-)}{S(E_+) + S(E_-)} = \frac{2\Delta E_y}{E_{0y}} \quad (\text{IV-16})$$

By adjustment of a resistor network in the E field pulser, we maintain $\Delta E_y < 2 \times 10^{-3} E_{0y}$.

2. Measurements with Linearly Polarized uv.

ΔE_z : This can be measured using linearly polarized light at 45° with respect to the \hat{y} axis. Let $\hat{\epsilon}_{\pm} = \frac{1}{\sqrt{2}} (\hat{y} \pm \hat{z})$. Then it can be shown that the signal sizes for the 0-1, 0-0 lines are:

$$S_{01}(\hat{\epsilon}_{\pm}) = \frac{\beta^2 E_y^2}{2} \left(1 \mp 2 \frac{E_z}{E_y} \right) \quad (\text{IV-17})$$

$$S_{00}(\hat{\epsilon}_{\pm}) = \frac{\alpha^2 E_y^2}{2} \left(1 \pm 2 \frac{E_z}{E_y} \right) \quad (\text{IV-18})$$

respectively. Forming the experimental asymmetries:

$$a(\epsilon_{\pm}) = \frac{S_{E+} - S_{E-}}{S_{E+} + S_{E-}}$$

where the subscripts E_{\pm} refer to electric field orientation, we find

$$\frac{\Delta E_z}{E_{0y}} = \left(\frac{1+f}{1-f} \right) \frac{a(\epsilon_+) - a(\epsilon_-)}{4} \quad (\text{IV-19})$$

E_{0z}/E_{0y} : The linear polarization experiment provides additional information through Δ_P . With $\hat{\epsilon}_{\pm} = \frac{1}{\sqrt{2}} (\hat{y} \pm \hat{z})$, we obtain:

$$\Delta_P = \frac{-2M}{\beta E_{0y}} \left(\theta_x + \frac{E_{0z}}{E_{0y}} \right) = \Delta_M \left(\theta_x + \frac{E_{0z}}{E_{0y}} \right) \quad (\text{IV-20})$$

where in (IV-20) only the most significant terms have been retained.

For $\theta_x = 0$, $\frac{E_{0z}}{E_{0y}} = \frac{\Delta_P}{\Delta_M}$. Since this formula applies to both blocked and

unblocked data we may use a weighted average of the two results to

obtain E_{0z}/E_{0y} . If we now employ a magnetic field $B_x = \pm 5$ gauss,

it is possible to determine θ_x for these fields. The result is θ_x

(5 gauss) = $0.22 \pm .01$.

3. Measurements Employing Magnetic Fields and Circularly Polarized Light

E_{0x}/E_{0y} : Returning to circular polarization but using the same magnetic fields we form the difference between $\Delta_E(+\theta_x)$ and $\Delta_E(-\theta_x)$ to eliminate terms independent of θ_x in Eq. (IV-15). Keeping only the significant term we find:

$$\frac{E_{0x}}{E_{0y}} = \frac{\Delta_E(+\theta_x) - \Delta_E(-\theta_x)}{4\theta_x} \quad (\text{IV-21})$$

$\Delta E_x/E_{0y}$ and $(n \sin \phi + n' \sin \phi')$: Forming a similar difference for Δ_p one finds:

$$\Delta_p(+\theta_x) - \Delta_p(-\theta_x) = 2\theta_x \left[\frac{2\Delta E_x}{E_{0y}} + \Delta_M (n \sin \phi + n' \sin \phi') \right] \quad (\text{IV-22})$$

By comparing this difference for blocked and unblocked data one obtains:

$$(n \sin \phi + n' \sin \phi') = \frac{[\Delta_{pb}(+\theta) - \Delta_{pb}(-\theta) - (\Delta_{pu}(+\theta) + \Delta_{pu}(-\theta))]}{2\theta_x (\Delta_{Mb} - \Delta_{Mu})} \quad (\text{IV-23})$$

$$\frac{\Delta E_x}{E_{0y}} = \frac{\Delta_{pb}(-\theta) - \Delta_{pb}(+\theta) - \frac{\Delta_{Mb}}{\Delta_{Mu}} (\Delta_{pu}(-\theta) - \Delta_{pu}(+\theta))}{2\theta_x \left(\frac{\Delta_{Mb}}{\Delta_{Mu}} - 1 \right)} \quad (\text{IV-24})$$

It should be noted that the measured $\frac{E_{0x}}{E_{0y}}$, $\frac{\Delta E_x}{E_{0y}}$, and $n \sin \phi + n' \sin \phi'$

are diluted by the same polarization analyzing power as Δ_p and Δ_M , whereas E_{0z}/E_{0y} and $\Delta E_z/E_{0y}$ are not. As a result, the various products of these terms appearing in Δ_{FALSE} (Eq. IV-13) all have the same dilutions as Δ_p . To summarize, all possible significant false parity asymmetries associated with imperfections in optical polarizations and the electro-magnetic fields appear in the foregoing analysis, and all terms have been measured by independent experiments.

V. DATA ANALYSIS AND RESULTS

A. Secondary Data Sets and Auxiliary Data

The sequence in which data are accumulated is shown in Table V.Ia. During one of these sets (which requires about 40 minutes) signal corrections (Eqs. IV-8, IV-9) and normalization are quite constant, since manual adjustments to the apparatus such as mirror rotation and balance of E field are generally done on a longer time scale.

We define a secondary data point as an average of 80 primary points (unblocked) and 48 primary points (blocked). One determines the average parity, MI and signal asymmetries, and signal sizes necessary to perform the corrections of Eqs. IV-8, IV-9. These corrections are calculated separately for each interaction region, averaged, and assigned a statistical uncertainty determined from the combined uncertainty of all the factors in Eqs. IV-8, IV-9. The net correction is subtracted from $\Delta_{p,obs}^i$ to obtain Δ_p^i while the uncertainties are combined in quadrature. Each of the Δ_p^i and associated uncertainties are then normalized to $\Delta_{M,b} = 9.0 \times 10^{-3}$ to account for the variations in analyzing power between secondary data points which affect parity and MI asymmetries in the same way. These variations are due to fluctuations in i.r. power and polarization, and changes in background and 0-0 dilution. A weighted average of the normalized Δ_p^i is then taken over a run (see Tables V.2, V.3).

Interspersed throughout a run at intervals of approximately 10 basic data sets, are sets of auxiliary measurements needed to determine E_{0x} , E_{0y} , ΔE_x , ΔE_z and $(n \sin \phi + n' \sin \phi')$. A typical sequence

Table V.1 Data Accumulation Sequences

a. 1. Secondary Parity Data Set

Circ Pol uv: $B_x = 0$ gauss

u u b u u b u ($B_u B_b$) b u b u u b u u b u u b u u b u ($B_u B_b$) b u b u u b u u b
 $\gg \ll 1 \text{ min}$

time \rightarrow

b) Calibration Data

1. Circ Pol. uv, $B_x = \pm 5$ gauss:

u b... (5 cycles) ($B_u B_b$) u b... (5 cycles)

2. Lin. Pol. uv, $B_x = 0$:

u b u b... (5 cycles) ($B_u B_b$) u b u b... (10 cycles) ($B_u B_b$)

u b u b... (5 cycles)

u: Signal + Background, unblocked

b: Signal + Background, blocked

B_u : Background, unblocked

B_b : Background, blocked

Each symbol (e.g., u) represents 4 primary data points,

(4 x 256 = 1024 pulses).

Table V.2 Parity Data with Mirror ("Unblocked")

| Run | (a) | (b) | SYSTEMATIC EFFECTS
($\times 10^{-7}$) | | | (f) | (g) | Weight |
|-----|---------------------------|----------------------|--|----------|----------|--------|---------------------------|--------|
| | $\Delta_p \times 10^{-7}$ | $r_p \times 10^{-7}$ | (c) | (d) | (e) | (f) | $\Delta_p \times 10^{-7}$ | |
| 1 | 261 | 159 ± 180 | 52 ± 47 | 14 ± 63 | -10 ± 8 | -3 ± 1 | 106 ± 197 | 2.564 |
| 2 | 91 | 195 ± 199 | -1 ± 13 | -30 ± 45 | -27 ± 7 | -1 ± 0 | 254 ± 265 | 2.379 |
| 3 | -244 | -103 ± 283 | -13 ± 30 | 2 ± 30 | -10 ± 9 | 0 ± 0 | -82 ± 286 | 1.220 |
| 4 | -141 | -62 ± 146 | 10 ± 15 | 30 ± 42 | -21 ± 9 | -1 ± 1 | -20 ± 153 | 4.276 |
| 5 | 272 | 270 ± 179 | 9 ± 23 | -22 ± 52 | -61 ± 15 | -1 ± 1 | 345 ± 188 | 2.817 |
| 6 | -221 | -171 ± 204 | 0 ± 3 | 2 ± 17 | -8 ± 13 | 0 ± 1 | -165 ± 205 | 2.376 |
| 7 | 192 | 49 ± 108 | -6 ± 8 | -25 ± 31 | -12 ± 8 | -1 ± 0 | 93 ± 113 | 7.841 |
| 8 | 22 | 124 ± 80 | -2 ± 5 | -11 ± 16 | -69 ± 19 | -1 ± 0 | 207 ± 84 | 14.201 |
| 9 | -63 | 15 ± 197 | 15 ± 21 | 74 ± 109 | -48 ± 19 | 1 ± 1 | -27 ± 227 | 1.942 |
| 10 | -141 | 160 ± 195 | 16 ± 25 | -59 ± 73 | -24 ± 12 | -1 ± 1 | 228 ± 210 | 2.266 |
| 11 | 107 | 302 ± 136 | -1 ± 13 | -43 ± 51 | -18 ± 10 | -1 ± 1 | 365 ± 146 | 4.680 |
| Av | 46 | 103 | 4 | -16 | -36 | -1 | 153 ± 45 | |

a) Uncorrected

b) Signal correction included (Eq'n IV-9)

c) $-(n \sin \phi + n') \frac{2M}{E_{Oy}} E_{Oz} / E_{Oy}$

d) $-2E_{Oz} \Delta \Gamma_x / E_{Oy}^2$

e) $-2E_{Ox} \Delta E_z / E_{Oy}^2$

f) $+4E_{Ox} E_{Oz} \Delta E_y / E_{Oy}^3$

g) Δ_p with all corrections.

Table V.3 Parity Data without Mirror ("Blocked")

| Run | (a) | (b) | SYSTEMATIC EFFECTS
($\times 10^{-7}$) | | | | (g) | Weight |
|-----|---------------------------|----------------------|--|--------------|--------------|------------|--------------------------------|--------|
| | $\Delta_p \times 10^{-7}$ | $b_p \times 10^{-7}$ | (c) | (d) | (e) | (f) | $b_p \times 10^{-7}$ | |
| 1 | 194 | 180 \pm 251 | 197 \pm 179 | 14 \pm 63 | -12 \pm 7 | -3 \pm 1 | -16 \pm 315 | 1.009 |
| 2 | -50 | -29 \pm 247 | -2 \pm 47 | -30 \pm 45 | -14 \pm 7 | 0 \pm 0 | 17 \pm 256 | 1.532 |
| 3 | 508 | 542 \pm 469 | -47 \pm 111 | 2 \pm 30 | -20 \pm 11 | 0 \pm 1 | 607 \pm 403 | .429 |
| 4 | 451 | 434 \pm 225 | 39 \pm 58 | -30 \pm 42 | -22 \pm 12 | -1 \pm 0 | 448 \pm 236 | 1.789 |
| 5 | 73 | 88 \pm 324 | 28 \pm 74 | -22 \pm 52 | -35 \pm 18 | -1 \pm 1 | 118 \pm 337 | .881 |
| 6 | -358 | -362 \pm 401 | 0 \pm 8 | 3 \pm 21 | -15 \pm 27 | 0 \pm 1 | -350 \pm 403 | .617 |
| 7 | 23 | 12 \pm 195 | -30 \pm 42 | -25 \pm 31 | -8 \pm 8 | -1 \pm 0 | 76 \pm 202 | 2.450 |
| 8 | 130 | 159 \pm 110 | -7 \pm 17 | -11 \pm 16 | -56 \pm 13 | -1 \pm 0 | 234 \pm 113 | 7.804 |
| 9 | 86 | 76 \pm 269 | 137 \pm 191 | 74 \pm 109 | -53 \pm 22 | 1 \pm 1 | -83 \pm 348 | .825 |
| 10 | -221 | -185 \pm 258 | 61 \pm 99 | -59 \pm 73 | -24 \pm 10 | -1 \pm 1 | -162 \pm 286 | 1.223 |
| 11 | 133 | 155 \pm 186 | -5 \pm 49 | -43 \pm 51 | -21 \pm 11 | -1 \pm 1 | 225 \pm 199 | 2.518 |
| Av | 104 | 118 | 15 | -10 | -33 | -1 | <u>155 \pm 58</u> | |

a) Uncorrected

b) Signal correction included (eq'n IV-8)

c) $-(n \sin \phi + n' \sin \phi') \frac{2H}{E_{Oy}} E_{Oz} / E_{Oy}$ d) $-2E_{Oz} \Delta E_x / E_{Oy}^2$ e) $-2E_{Ox} \Delta E_z / E_{Oy}^2$ f) $+4E_{Ox} E_{Oz} \Delta E_y / E_{Oy}^3$ g) Δ_p with all correction

Table V.4 Results of Auxiliary Measurements

| Run | (a) | (b) | (c) | (d) | (e) | (f) | (g) |
|-----|-----------|----------|--------|--------|---------|---------|---------|
| 1 | 210 ± 102 | 103 ± 43 | 20 ± 2 | 22 ± 2 | 17 ± 11 | 22 ± 10 | -5 ± 19 |
| 2 | -2 ± 45 | 116 ± 42 | 20 ± 2 | 23 ± 2 | 48 ± 9 | 28 ± 12 | 10 ± 11 |
| 3 | -99 ± 97 | 53 ± 73 | 19 ± 2 | 12 ± 2 | 32 ± 25 | 42 ± 17 | -1 ± 20 |
| 4 | 80 ± 51 | 54 ± 45 | 26 ± 2 | 27 ± 2 | 30 ± 11 | 34 ± 16 | 22 ± 12 |
| 5 | 36 ± 69 | 86 ± 62 | 26 ± 2 | 28 ± 2 | 83 ± 14 | 51 ± 22 | 9 ± 16 |
| 6 | 1 ± 73 | -12 ± 63 | 41 ± 3 | 41 ± 2 | 10 ± 16 | 16 ± 26 | 10 ± 18 |
| 7 | -39 ± 35 | 85 ± 43 | 23 ± 1 | 22 ± 1 | 22 ± 12 | 14 ± 13 | 12 ± 8 |
| 8 | -14 ± 27 | 51 ± 36 | 33 ± 2 | 33 ± 2 | 83 ± 19 | 67 ± 12 | 8 ± 6 |
| 9 | -173 ± 69 | -88 ± 87 | 26 ± 2 | 24 ± 2 | 70 ± 23 | 71 ± 24 | 29 ± 14 |
| 10 | 43 ± 53 | 158 ± 61 | 17 ± 2 | 21 ± 1 | 44 ± 18 | 54 ± 18 | 14 ± 12 |
| 11 | -5 ± 42 | 124 ± 46 | 20 ± 1 | 22 ± 1 | 31 ± 15 | 40 ± 17 | 13 ± 10 |

a) $(n \sin \phi + n' \sin \phi') \times 10^{-3}$

b) $E_{0z}/E_{0y} \times 10^{-4}$

c) $(E_{0x}/E_{0y})_b \times 10^{-4}$

d) $(E_{0x}/E_{0y})_u \times 10^{-4}$

e) $(\Delta E_z/E_{0y})_u \times 10^{-5}$

f) $(\Delta E_z/E_{0y})_b \times 10^{-5}$

g) $\Delta E_x/E_{0y} \times 10^{-5}$

of auxiliary measurements is shown in Table V.1b. In a typical run, there are about 6 such sequences. These measurements must also be corrected with Eqs. I'7-8, IV-9. In addition, measurements with $B_x \neq 0$ must be corrected for hyperfine mixing (see Section IV.D). With these precautions E_{0x} , E_{0z} , ΔE_z , and $n \sin \phi + n' \sin \phi'$ can be extracted reliably and precisely.

Results of the auxiliary measurements are displayed by run in Table V.4. Quantities ΔE_x , and ΔE_z are fairly constant from first to last run, although perhaps they show a slight increase with time (as the cell degraded gradually). The values of E_x and E_z also remain fairly constant except for deviations associated with adjustments of angles and positions of L1 and L2 laser beams. The quantity $n \sin \phi + n' \sin \phi'$ varies more erratically from run to run, since it depends sensitively on Pockels cell alignment, which was reset for each run. There is no indication of variation between re-alignments. The net contribution from this term averaged over all runs is small.

B. Results

The normalized average corrections for a given run are subtracted from the weighted average of the normalized Δ_p^i . The statistical uncertainty associated with each correction is combined in quadrature with the statistical uncertainty in the normalized Δ_p^i , for this run. This, finally, is a measurement of the parity asymmetry with associated statistical uncertainty. Our total data sample consists of 11 such runs, listed in Tables V.2, V.3. A weighted average yields

Table V.5 Correlation Tests(a)

| Results for 425 Second-Order Data Points(b) | | | |
|---|-----------------------------|-------|----------------------|
| x(c) | y(c) | R(d) | p(e) |
| $\Delta_{pu,r}$ | t(f) | .039 | .42 |
| $\Delta_{pu,s}$ | t(f) | -.019 | .70 |
| $\Delta_{pb,r}$ | t(f) | -.014 | .77 |
| $\Delta_{pb,s}$ | t(f) | -.014 | .77 |
| $\Delta_{pu,s}$ | $\Gamma_b - \Gamma_u$ | .239 | 6.5×10^{-7} |
| $\Delta_{pu,s}$ | $\Gamma_b - \Gamma_u$ | -.103 | 3.4×10^{-2} |
| $\Delta_{pb,r}$ | Γ_b | .109 | 2.5×10^{-2} |
| $\Delta_{pb,s}$ | Γ_b | .048 | .32 |
| $\Delta_{pu,s}$ | $\Gamma_{u1} - \Gamma_{u2}$ | .019 | .70 |
| $\Delta_{pb,s}$ | $\Gamma_{u1} - \Gamma_{u2}$ | -.006 | .90 |
| $\Delta_{pu,s}$ | $\Delta_{E,u}$ | .036 | .46 |
| $\Delta_{pb,s}$ | $\Delta_{E,b}$ | -.058 | .23 |
| $\Delta_{pu,r}$ | Γ_u | .042 | .39 |
| $\Delta_{pu,s}$ | Γ_u | -.046 | .34 |
| $\Delta_{pu,s}$ | $\Delta_{pb,s}$ | -.025 | .61 |
| $\Delta_{pu,r}$ | $\sigma_{u,r}$ | .039 | .42 |
| $\Delta_{pu,s}$ | $\sigma_{u,s}$ | .000 | 1.0 |
| $\Delta_{pb,r}$ | $\sigma_{b,r}$ | .089 | 6.7×10^{-2} |
| $\Delta_{pb,s}$ | $\sigma_{b,s}$ | .066 | .17 |
| $\Delta_{pu,r}$ | Δ_{Mb} | .026 | .59 |
| $\Delta_{pu,s}$ | Δ_{Mb} | .041 | .40 |
| $\Delta_{pb,r}$ | Δ_{Mb} | .003 | .95 |
| $\Delta_{pb,s}$ | Δ_{Mb} | .028 | .56 |
| σ_M | Δ_{Mb} | -.041 | .40 |

(Table V.5; Continued)

- (a) See Section IV.C
 (b) Secondary Data point defined in Section V.A
 (c) Subscript r: uncorrected; s: corrected
 (d)

$$R = \frac{\left(\sum_i \frac{1}{\sigma_i^2}\right) \left(\sum_i \frac{x_i y_i}{\sigma_i^2}\right) - \left(\sum_i \frac{x_i}{\sigma_i^2}\right) \left(\sum_i \frac{y_i}{\sigma_i^2}\right)}{\left\{ \left[\left(\sum_i \frac{1}{\sigma_i^2}\right) \left(\sum_i \frac{x_i^2}{\sigma_i^2}\right) \left(\sum_i \frac{x_i}{\sigma_i^2}\right)^2 \right] \times \left[\sum_i \frac{1}{\sigma_i^2} \sum_i \frac{y_i^2}{\sigma_i^2} - \left(\sum_i \frac{y_i}{\sigma_i^2}\right)^2 \right] \right\}^{1/2}}$$

- (e) P = probability that the 2 data sets come from uncorrelated parent populations.
 (f) "Time" correlation = correlations between successive secondary data points.

$$\Delta_{pb} = 1.55 \pm 0.58 \times 10^{-5} \quad (V-1)$$

$$\Delta_{pu} = 1.53 \pm 0.45 \times 10^{-5} \quad (V-2)$$

The data were also treated by applying the field corrections to each secondary data point and then combining. The results of this method are very close to the values quoted.

C. Correlation Tests

A correlation study was done on the set of 425 secondary data points, both before and after corrections were applied, to examine the possible dependence of Δ_p on other system parameters (see Table v.5). Before corrections one finds a high correlation between $\Delta_{p,u}$ and $\Gamma_b - \Gamma_u$ (see eqn. IV-9) as well as between $\Delta_{p,b}$ and Γ_b (see eq. IV-8). The only significant correlation surviving after the corrections is between $\Delta_{p,u}$ and $\Gamma_b - \Gamma_u$, and it has reversed sign. This suggests that the correction of Eq. IV-9 has been over-estimated (by about 30 percent). We believe that this is largely due to reflections in the cell, which can only be estimated crudely. Therefore we average the results of our model (Eq. IV-9) and the predictions of the correlation study, and expand the systematic error to include both possibilities. This lowers the average of $\Delta_{p,u}$ by 0.10×10^{-5} from that originally calculated. All other correlations with the corrected data are at an acceptable low level.

D. Systematic Uncertainties and Final Results

The systematic uncertainties are summarized in Table V6. Since the sources of these systematic effects are uncorrelated, we combine the uncertainties in quadrature. The final results are:

$$\Delta_{p,b} = (1.55 \pm 0.58 \pm .06) \times 10^{-5} \quad (V-3)$$

$$\Delta_{p,u} = (1.43 \pm 0.45 \pm 0.11) \times 10^{-5} \quad (V-4)$$

where the first uncertainty in each equation is statistical and the second is systematic. Since these results are consistent they may be combined to yield the result:

$$\Delta_p = (1.48 \pm 0.36 \pm 0.09) \times 10^{-5} \quad (V-5)$$

The corrected result for data taken on the 0-0 line is $\Delta_{00} = - (0.13 \pm 0.82 \pm 0.02) \times 10^{-5}$, where no $7^2P_{1/2}$ polar² expected.

In order to compare with theory we calculate $\delta = 2 \operatorname{Im} \epsilon_p / M$. We take the ratio $2 \Delta_p(0-1) / \Delta_M'$ where $\Delta_M' = 9.0 \times 10^{-3} K$. The factor K corrects for reflections from the rear of the main cell, which reduces Δ_M but not Δ_p . We estimate $K = 1.17$, but it might be somewhat smaller, which leads to a skewness in our final result,

$$\delta = (2.8 \pm .7 \begin{matrix} +.3 \\ -.2 \end{matrix}) \times 10^{-3} \quad (V-6)$$

This result is consistent with theory (see Eq. II-20).

Table V.6 Systematic Uncertainties

| Source | Possible Contribution to: | |
|--|---------------------------|------------------------|
| | Δ_{Pb} | Δ_{Pu} |
| Uncorrected Signal Asymmetries: | $< 2 \times 10^{-8}$ | $< 2 \times 10^{-8}$ |
| Hyperfine Mixing: | $< 4 \times 10^{-8}$ | $< 1 \times 10^{-8}$ |
| E - uv correlation: | $< 1 \times 10^{-7}$ | $< 3 \times 10^{-8}$ |
| E_z (Imperfect cancellation of residual B_x): | $< 4 \times 10^{-7}$ | $< 3 \times 10^{-7}$ |
| ΔE_z (Imperfect uv, E subtraction): | $< 4 \times 10^{-7}$ | $< 4 \times 10^{-7}$ |
| E_x (Misaligned B_x and possible admixture of 1-1 line): | $< 7 \times 10^{-8}$ | $< 7 \times 10^{-8}$ |
| ΔE_x (Failure of approximation that effect is same with and without mirror): | $< 1 \times 10^{-7}$ | $< 1 \times 10^{-7}$ |
| Same as previous item for $n \sin + n' \sin \phi'$: | $< 1 \times 10^{-7}$ | $< 3 \times 10^{-8}$ |
| Signal corrections: ^(a) | $< 2 \times 10^{-7}$ | $< 1 \times 10^{-6}$ |
| Totals combined in quadrature: | $< 6 \times 10^{-7}$ | $< 1.1 \times 10^{-6}$ |
| Dilution due to uv polarization imperfections: ^(b) | $< 2 \times 10^{-7}$ | $< 2 \times 10^{-7}$ |

(a) See Section V.C

(b) This effect can only reduce the observed asymmetry.

VI. COMPARISON TO OTHER EXPERIMENTS AND THEORIES

Other efforts are currently underway to observe atomic parity non-conservation in hydrogen, cesium, and bismuth. These atoms have been listed in order of decreasing experimental difficulty and theoretical confidence.

The hydrogen experiments are being pursued in Seattle (Tra 79), Michigan (Dun 78), and Yale (Hin 79). These experiments offer not only a high degree of theoretical confidence but also allow observation of C_{1p} , C_{2n} , and C_{2p} in addition to C_{1n} . The experiments are however very difficult, if possible, and results are years away (Com 80).

The cesium 6S-7S transition is being pursued in laboratories in Paris (Bou 76, Bou 79b) as well as in Michigan and Zurich. The asymmetry is approximately one order of magnitude smaller than that in thallium. The fractional calculational uncertainties are comparable to those in thallium (see Table VI.1). Results here should be available soon and should provide a test of quark couplings comparable to those obtained in thallium.

Optical rotation experiments in bismuth are being pursued in Seattle, Oxford, Moscow, and Novosibirsk. Seattle (Lew 77) and Oxford (Bai 77) originally reported null results. Novosibirsk (Bar 79) subsequently reported observation of optical rotation consistent with their predictions based on the Weinberg-Salam model. Currently, Seattle and Oxford also claim to be seeing optical rotations consistent with their predictions based on the Weinberg-Salam model.

Their predictions and experiments are, however, in disagreement with the Novosibirsk result. Recently, Moscow (Bog 80) reported that they see no evidence for any rotation. These results are listed along with theoretical predictions in Table (VI.2, VI.3). The presence of three valence electrons in bismuth makes the atomic calculations difficult, accounting for the broad range of theoretical predictions. Hopefully, the theoretical and experimental discrepancies in bismuth will soon be resolved. However, at present it is impossible to place any meaningful restrictions on the quark coupling constants from the bismuth results.

Table VI.1. Calculation of ϵ_p and δ in Cesium and Thallium for $\sin^2\theta_w = .23$ (Com 80)

| Atom | Transition | Ref. | $\text{Im}(\epsilon_p) \times 10^{10} \text{ au.}$ | $\delta = 2\text{Im}(\epsilon_p)/M$ |
|------|-------------------------------------|------------------|--|-------------------------------------|
| Cs | $6^2S_{1/2} \rightarrow 7^2S_{1/2}$ | (Bou 74b,75a) | -12 | |
| | | (Lov 75, Bri 76) | -15 | |
| | | (Neu 77b)* | -09 | |
| Tl | $6^2P_{1/2} \rightarrow 7^2P_{1/2}$ | (Sus 76) | -76 | |
| | | (Neu 77a)* | -83 | 2.2×10^{-3} |
| | | Present Result* | -70 | 1.9×10^{-3} |
| | $6^2P_{1/2} \rightarrow 6^2P_{3/2}$ | (Neu 76) | -3.3 | |
| | | (Neu 77a)* | -3.5 | |
| | | (Hen 76) | -4.04 | |
| | (Hen 77) | -2.76 | | |
| | $6^2P_{1/2} \rightarrow 7^2P_{3/2}$ | (Neu 77a)* | .76 | |

*Indicates continuum and auto-ionizing contributions included.

Table VI.2 Calculation of Optical Rotation in Bismuth with $\sin^2\theta_W = .23$ (San 80a)

| Method | Ref. | 10^8R (876 nm) | 10^8R (648 nm) |
|--|----------|------------------|------------------|
| Central Field* | (Hen 76) | -17 | |
| Central Field* | (Har 78) | -17 | -22 |
| Hartree-Fock* | (Car 79) | -16 | -21 |
| Semi-Empirical | (Nov 76) | -13 | -17 |
| Parametric Potential
with Shielding and
first order
perturbations | (Har 78) | -11 | -13 |
| H-F with Shielding | (Mar 81) | -8 | -11 |

* Indicates calculation does not go beyond the independent particle model.

Table VI.3 Results of Optical Rotation Experiments in Bismuth

| Transition | Ref. | 10^8R |
|------------|-----------|-----------------|
| 876 nm | (Lew 77) | $-.7 \pm 3.2$ |
| 876 nm | (Hol 81) | -10.4 ± 1.7 |
| 648 nm | (Bai 77) | 2.7 ± 4.7 |
| 638 nm | (Bar 79) | -20.6 ± 3.2 |
| 648 nm | (Bog 80) | 2.3 ± 1.3 |
| 648 nm | (San 80b) | -10.3 ± 1.8 |

VII. CONCLUSIONS

Our results (eqn. V-6) may be expressed in terms of Q_W , using eqs. II-18, II-19, and II-20 we find:

$$Q_{W, \text{expt}}(T1) = -197 \pm 111 \quad (\text{VII-1})$$

where the uncertainty includes that in $(\epsilon_p)_{\text{theo}}$ as well as the uncertainty in ϵ_{expt} .

The results of the electron scattering experiment and the present experiment in T1 may be combined with neutrino-nucleon and neutrino-electron scattering data to provide a stringent test of neutral weak interaction theories. In carrying out this analysis it is useful to employ the simplest model-independent assumptions, as was done by Hung and Sakurai (Hun 79). They show that if one merely assumes μe universality, that the contributions of heavy quarks, c, s, \dots may be neglected, and that all neutral weak currents possess only V and A components, then the theory is characterized by 10 coupling constants $\tilde{\alpha}, \tilde{\beta}, \tilde{\gamma}, \tilde{\delta}, \alpha, \beta, \gamma, \delta, g_V$ and g_A , which must be determined by experiment. The neutrino-nucleon scattering data completely determine α, β, γ , and δ (up to an overall sign ambiguity), while neutrino-electron scattering results determine g_V, g_A up to a (two-fold) V,A ambiguity. The polarized electron scattering experiment (Pre 78, 79) yields:

$$\tilde{\alpha} + \frac{1}{3} \tilde{\gamma} = -0.60 \pm 0.16, \quad \tilde{\beta} + \frac{1}{3} \tilde{\delta} = 0.31 \pm 0.51 \quad (\text{VII-2})$$

Our experiment is sensitive to an almost orthogonal linear combination of $\tilde{\alpha}$ and $\tilde{\gamma}$:

$$Q_W(T1) = 42\tilde{\alpha} - 612\tilde{\gamma} \quad (\text{VII-3})$$

As Hung and Sakurai have noted, further restrictions on the coupling constants are obtained if one assumes the "factorization" hypothesis. Employing result (VII-1), formula (VII-3), and factorization we represent the resulting constraints on $\tilde{\alpha}$ and $\tilde{\gamma}$ in Fig. VII-1 and obtain:

$$\tilde{\alpha} = -.67 \pm 0.16 \quad (\text{VII-4})$$

$$\tilde{\gamma} = +0.18 \pm 0.06 \quad (\text{VII-5})$$

Assuming factorization, Hung and Sakurai show that all 10 constants are determined without ambiguities and are in excellent agreement with predictions of the standard model for $\sin^2 \theta_W = 0.23$. Without factorization $\tilde{\beta}$ and $\tilde{\delta}$ remain undetermined experimentally.

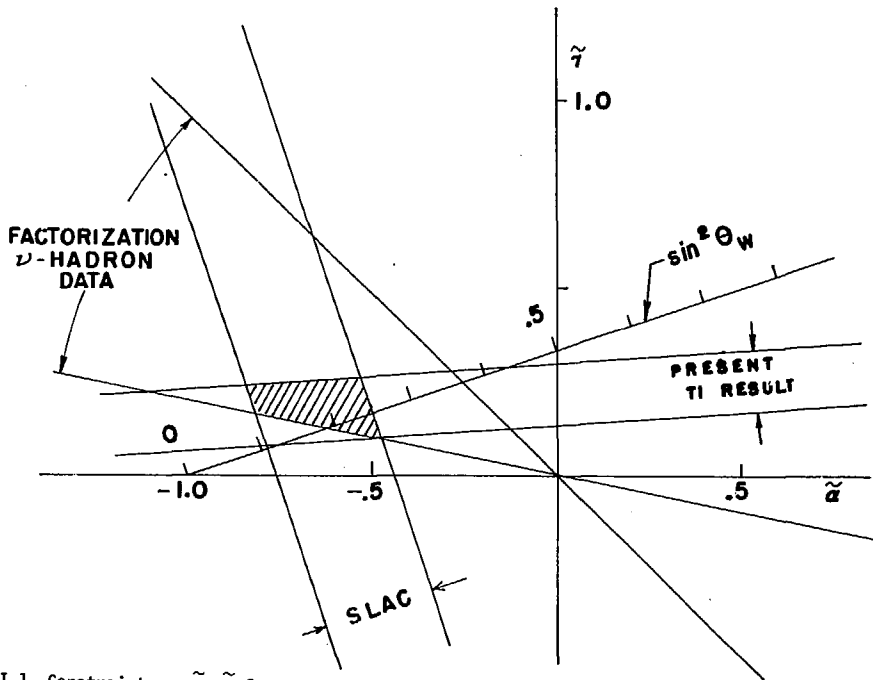


Figure VII.1 Constraints on $\tilde{\alpha}$, $\tilde{\gamma}$ from: ν -Hadron scattering (factorization hypothesis); XBL 811-7637 SLAC polarized electron experiment; Results of the present T1 experiment. The region of the $\tilde{\alpha}$, $\tilde{\gamma}$ plane consistent with all of these constraints is cross-hatched. This fig. was calculated with $\delta_{\text{Theo}} = (2.1 \pm 0.7) \times 10^{-3}$.

VIII. FUTURE WORK

A substantial improvement in the measurement of $\text{Im}(\epsilon_p)/\beta$ for the $6^2P_{1/2} - 7^2P_{1/2}$ transition in Tl seems possible by means of a technique utilizing linearly polarized 293 nm light and an external magnetic field. This experiment, currently being pursued in our laboratory, is sensitive to a completely different pseudoscalar, proportional to

$$\hat{\mathbf{k}} \cdot \vec{\mathbf{B}} \cdot \hat{\mathbf{e}} \vec{\mathbf{E}} \times \vec{\mathbf{B}}$$

where $\hat{\mathbf{k}}$ is chosen parallel to $\vec{\mathbf{E}}$ and $\hat{\mathbf{e}}$ is the polarization vector of the incident laser light. This technique might also be applied to the $6S_{1/2} - 7S_{1/2}$ or $6S_{1/2} - 8S_{1/2}$ transitions in cesium (Bou 79). An alternative approach involving an initial polarization of the ground state may also hold future promise for these transitions. A direct measurement of α and/or β seem feasible and would provide a useful test of the perturbation formalism used in the calculation of α , β , and ϵ_p .

The more long range goals for parity nonconservation in atoms should focus on experiments to place limits on $\tilde{\beta}$ and $\tilde{\delta}$. These experiments will need to be orders of magnitude more sensitive than current experiments in order to observe the coupling of the axial nucleonic current to the vector electronic current.

REFERENCES

- (Abb 78) L. F. Abbott and R. M. Barnett, Phys. Rev Lett. 40, 1303 (1978).
- (Abe 73) E. S. Abers and B. W. Lee, Phys. Lett. C., 9C, 1.
- (Bai 77) P.E.G. Baird, M.W.S.M. Brimicombe, R. G. Hunt, G. J. Roberts, P.G.H. Sandars, P. N. Stacy, Phys. Rev. Lett. 39, 798.
- (Bar 79) L. M. Barkov, N. S. Zolotarev, JETP Lett. 27, 357 and also Phys. Lett. 85B, 308.
- (Bar 80) J. N Bardsley and D. W. Norcross, J.Q.S.R.T. 23, 575.
- (Bel 79) J. S. Bell, 1979, Proc. Workshop on Parity Violation in Atoms (Cargese), in press.
- (Bog 80) Y. V. Bogdanov et al., Preprint No. 43, Quantum Physics Institute, P. N. Lebedev Institute, Acad. Sci. USSR, Moscow.
- (Bou 74a) M. A. Bouchiat and C. Bouchiat, Phys. Lett., 40B, 111.
- (Bou 74b) M. A. Bouchiat and C. Bouchiat, J. de Physique, 35, 889.
- (Bou 75a) M. A. Bouchiat and C. Bouchiat, J. de Physique, 36, 493.
- (Bou 75b) M. A. Bouchiat and L. Pottier, J. de Physique Lett., 36, L-189.
- (Bou 76) M. A. Bouchiat and L. Pottier, J. Phys. Lett. (Paris) 37, L79.
- (Bou 79a) M. A. Bouchiat, M. Poitier, and C. Bouchiat, J. de Physique, 40, 1127.
- (Bou 79b) M. A. Bouchiat and L. Pottier, see Bell, 1979 in press.
- (Bou 80) M. A. Bouchiat, J. Guena, and L. Pottier, J. Phys. Lett. (Paris) 41, L-299.
- (Bri 76) M.W.S.M. Brimicombe, C. E. Loving, P.G.H. Sandars, J. Phys. B., 9, L237.
- (Buc 80) P. Bucksbaum, Ph.D. Thesis (Lawrence Berkeley Laboratory Publication LBL-11641).
- (Car 79) S. L. Carter, H. P. Kelley, Phys. Rev. Lett. 42, 966.

- (Chu 77) S. Chu, R. Conti, and E. Commins, Phys. Lett. A 60A, 96.
- (Chu 79) S. Chu and, R. W. Smith, Opt. Commun. 28, 221.
- (Com 80) E. Commins and P. Bucksbaum, Annual Review of Nuclear and Particle Science 30, 1.
- (Con 79a) R. Conti, P. Bucksbaum, S. Chu, E. Commins, and L. Hunter, Phys. Rev. Lett. 42, 343.
- (Con 79b) R. Conti, Ph.D. Thesis (unpublished)
- (Dun 78) R. W. Dunford, R. R. Lewis, W. L. Williams, Phys. Rev. A. 18, 2421.
- (Fai 76) H. Faissner, Report to 18th International Conference on High Energy Physics, Tbilisi, USSR.
- (Flu 76) A. Flusberg, T. Mossberg, and S. Hartmann, Phys. Rev. A14, 2146.
- (Gal 64) A. Gallagher and A. Lurio, Phys. Rev 136, A87.
- (Gou 70) H. Gould, Phys. Rev. Lett., 24, 1091.
- (Gra 79) I. P. Grant, S. J. Rose, P.G.H. Sandars, in press.
- (Har 78) M. J. Harris, C. E. Loving, P.G.H. Sandars, J. Phys. B. 11, L749.
- (Has 73) F. J. Hasert et al., Phys. Lett. 46B, 138.
- (Hen 76) E. M. Henley, L. Willets, Phys. Rev. A. 14, 1411.
- (Hen 77) E. M. Henley, M. Klapisch, L. Wilits, Phys. Rev. Lett. 39, 994.
- (Hin 76) E. A. Hinds, C. E. Loving, and P.G.H. Sandars, Phys. Lett. 62B, 97.
- (Hin 79) E. A. Hinds, see Bell, in press.
- (Hol 81) J. H. Hollister, G. R. Apperson, L. L. Lewis, T. P. Emmons, T. G. Vold, and E. N. Fortson, Phys. Rev. Lett. 46, 643.
- (Hun 79) P. Q. Hung and J. J Sakurai, Phys. Lett. 88B, 91.
- (Kas 48) M. Kasha, J Opt. Soc. 38, 929.
- (Khr 76) I. B. Khriplovich, V. N. Novikov, and D. P. Sushkov, Sov. Phys. JETP 44, 872.

- (Lew 77) L. L. Lewis, J. H. Hollister, D. C. Soreide, E. G. Lindahl and E. N. Fortson, *Phys. Rev. Lett.* 39, 795.
- (Lov 75) C. E. Loving and P.G.H. Sandars, *J. Phys. B.* 8, L336.
- (Mar 81) A. M. Martesson, E. M. Henley, and L. Wilets, to be published.
- (Mus 76) P. Musset, Report to 18th International Conference on High Energy Physics, Tbilisi, USSR.
- (Neu 77a) D. Neuffer and E. Commins, *Phys. Rev.* A16, 844.
- (Neu 77b) D. Neuffer and E. Commins, *Phys. Rev.* A16, 1760.
- (Nov 76) V. N. Novikov, O. P. Sushkov, I. B. Khriplovich, *Sov. Phys. (JETP)* 44, 872.
- (Pla 70) M. A. Player and P.G.H. Sandars, *J. of Physics*, B3, 1620.
- (Pre 78) C. Y. Prescott et al., *Phys. Lett.* 77B, 347.
- (Rei 76) F. Reines, H. S. Gurr, H. W. Sobel, *Phys. Rev. Lett* 37, 315.
- (Sal 68) A. Salam, in *Elem. Particle Theory*, ed. N. Svartholm (Almqvist and Forlag, Stockholm).
- (San 80a) P.G.H. Sandars, *Phys. Scr.* 21, 284.
- (San 80b) P.G.H. Sandars, Private Communication.
- (Sus 76) O. P. Sushkov, V. V. Flambaum, I. B. Khriplovich, *JETP Lett.* 24, 461.
- (Tra 79) T. Trainor, see Bell, 1979.
- (Wei 67) S. Weinberg, *Phys. Rev. Lett.*, 19, 1264.
- (Wei 74) S. Weinberg, *Rev. Mod. Phys.* 46, 255.
- (Zel 59) Ia B. Zel'dovich, *JETP*, 36, 964.